Received: 1 July 2025 | Revised: 12 February 2026 | Accepted: 24 February 2026

DOI: 10.1002/esp.70271

RESEARCH ARTICLE

ESPL WILEY

Flexible patchy vegetation in a meandering bend: Effect on main flow and dispersion processes

Donatella Termini | **Nina Benistati**

Department of Engineering, University of Palermo, Italy

Correspondence
Donatella Termini, Department of Engineering, University of Palermo, Italy.
Email: donatella.termini@unipa.it

Funding information
No funding was received for this study.

Abstract

The presence of submerged vegetated islands on riverbeds influences hydrodynamics in aquatic ecosystems. A better understanding of interactions between the vegetated islands and the neighboring flow is crucial, especially in river restoration. While most studies in this field refer to straight channels—which are relatively rare in nature—and to emergent rigid vegetation, in this study we focus on river bends with finite vegetation patches, particularly flexible and submerged. The analysis is performed with the aid of data collected in a high-sinuosity meandering flume with squared patches (percentage of coverage of 10%) of fully submerged flexible vegetation (Cauchy number $Ca = 14.5$) on the bed. Attention is focused on the bend-apex area of the flume. Results indicate the formation of a reduced-velocity region downstream of each patch's exit edge, along with a reverse flow on the vertical plane. In contrast to what is observed in straight channels, the extension of this region decreases as the local radius of curvature decreases. High values of the Reynolds stress and the turbulent kinetic energy clearly occur especially close to the lateral edges of the patches, where the vegetation becomes a sink of turbulent motion. The presence of vegetated patches alters the typical curvature-induced circulation motion and the streamwise velocity distribution at the apex section. Two cores of high velocity form in the central part of the water depth and accelerated streamwise flow velocities are clearly visible between the two patches. This pattern influences the exchange and dispersion processes not only within the vegetated areas but also in the lateral patch-adjacent area.

KEYWORDS
curved channels, experiments, Rivers, vegetation, velocity

1 | INTRODUCTION

Vegetation exerts a strong influence on the aquatic ecosystem, interacting with flow at different spatial scales (Nepf, 2012; Nikora, 2010) and exerting multiple services (Schulz et al., 2003). In a context of climate change, understanding flow-vegetation interaction processes is especially important in river restoration and for defining nature-based strategies (Termini, 2015a).

On one hand, by modifying the mean and turbulent flow fields, vegetation increases flow resistance and reduces the conveyance capacity (Biggs et al., 2019; Wu et al., 1999), influences the sediment transport processes (Gacia & Duarte, 2001; Schulz et al., 2003; Vargas-Luna et al., 2015), and alters the deposition/erosion processes along the channel (Follett & Nepf, 2012; Fonseca et al., 1983; Rominger & Nepf, 2011), playing a fundamental role in river's evolution. On the other hand, by influencing the mixing and exchange processes, vegetation affects the distribution of nutrients and oxygen (Tseng & Tinoco, 2024), modifies the residence time of pollutants and sediment (Liu et al., 2020; Lozovik et al., 2019), and consequently influences the quality conditions of the aquatic environment (Cotton et al., 2006; Mars et al., 1999; Pan et al., 2023; Schulz et al., 2003; Widdows et al., 2008; Wilcock et al., 1999; Windham et al., 2003; You & Zhang, 2017; Zhu et al., 2016). Vegetation also reduces the stressful conditions of the habitat and increases biodiversity

(Cornacchia et al., 2018), providing food and shelter for other organisms (Barsu et al., 2016; Figueiredo et al., 2015; Franklin et al., 2008; Liu & Wang, 2024), limiting the colonization by large organisms in the water column (Biggs, 1996), promoting the deposition of nutrient-rich fine sediment (Cotton et al., 2006; Sand-Jensen, 1998; Wharton et al., 2006), influencing macroinvertebrates living in velocity gradient areas (Bahmanpouri et al., 2022; Statzner et al., 1988), and supporting microbial activity (Caffrey & Kemp, 1992). Thus, understanding flow velocity patterns, transport and diffusion processes in the presence of vegetation is crucial for evaluating the status of the aquatic ecosystem.

In the past decades the analysis of flow-vegetation interactions in rivers has attracted a lot of attention from the scientific community. Several experimental studies performed in laboratory vegetated flumes have led significant advances in flow characteristics and transport processes (e.g., De Serio et al., 2018; Liu et al., 2018; Nepf, 1999; Poggi et al., 2004; Stone & Shen, 2002; Tanino & Nepf, 2008; Tseng & Tinoco, 2024; Wang et al., 2024; Zhao & Nepf, 2024). Most studies consider rigid vegetation, modeled by circular cylinders regularly or randomly distributed on the entire flume, in emergent condition (among others Rowi'nski & Kubrak, 2002; White & Nepf, 2007; Tan et al., 2019) and, in a lower number of cases, in submerged condition (e.g., Chen et al., 2011; Luhar & Nepf, 2011; Nepf & Vivoni, 2000; Zhao & Nepf, 2024). These studies indicate that, while in the emergent condition the primary source of turbulence comes from the stem wakes (Nepf & Vivoni, 2000), in the submergent condition a shear layer forms at the top of vegetation, the Kelvin-Helmholtz instability (among others Carollo et al., 2002, 2007; Ghisalberti & Nepf, 2006; Huai et al., 2009; Okamoto & Nezu, 2013; Termini, 2019) leads to the formation of large-scale turbulent coherent motion which enhances the vertical mixing and transport of nutrients and sediments (Ghisalberti & Nepf, 2006; Nezu & Sanjou, 2008; Termini, 2015b; Tseng & Tinoco, 2021). If the submerged vegetation is flexible, as the herbaceous one, a waving motion, called "monami" (Ackerman & Okubo, 1993), is associated with the passage of the turbulent coherent structures (Ghisalberti & Nepf, 2002; Nepf, 2012; Järvelä, 2002; Carollo et al., 2002, 2008; Termini, 2016). According to recent studies conducted by Cornacchia et al. (2018), such waving motion could inhibit vegetation growth by influencing the blade-to-blade interactions and hereby exerting an important role in ecosystem structure and function and habitat conditions (Bornette et al., 1998; Nikora, 2010).

In natural rivers, submerged herbaceous vegetation often grows in relatively well-defined areas (patches) of limited width and length rather than uniformly distributed on the bed (Forman, 1995; Sand-Jensen & Pedersen, 2008; Sand-Jensen & Vindboek Madsen, 1992; Schoelynck et al., 2012; Schoelynck et al., 2018; Biggs et al., 2019). The interactions between vegetated patches and the neighboring flow directly influence transport and exchange processes (Medjnoun et al., 2020), whose characteristics and magnitude are strongly controlled by the patches' dimensions (i.e., width and length) and their overall coverage percentage (Afzalimehr et al., 2021; Follet and Nepf, 2012; Huai et al., 2021; Kazem et al., 2021; Okamoto & Nezu, 2013). As an example, Kazem et al. (2021) established that a vegetation coverage of 10–40% (i.e., an intermediate coverage) may promote high species richness due to the conditions provided for fauna habitat (Killgore et al., 1993; Looby et al., 2021).

Despite their importance in nature, researchers devoted more attention to partly vegetated conditions only in the last decade (among others Zong & Nepf, 2012, Ortiz et al., 2013; Manners et al., 2015; Bywater-Reyes et al., 2018; Devi et al., 2019; Biggs et al., 2019; Przyborowski & Łoboda, 2021; Tranmer et al., 2024; Park & Nepf, 2025) so that the flow-vegetation interaction at the patch scale is not yet well known. While the major part of these studies consider channels partially covered with rigid emergent vegetation (e.g., Devi et al., 2019; Zong & Nepf, 2010) or distributed within finite patches (e.g., Tranmer et al., 2024; Zong & Nepf, 2012), few studies consider submerged vegetated patches and even less flexible vegetation, either arranged with a staggered pattern (Manners et al., 2015; Siniscalchi et al., 2012) or combined in groups (Devi & Kumar, 2016; Kazem et al., 2021; Przyborowski & Łoboda, 2021; Park & Nepf, 2025). In the presence of submerged vegetated patches, a complicated 3D flow structure generates between regions above and within vegetation (Siniscalchi et al., 2012), extending downstream of the patch for a length that depends on the patch's dimensions (Kazem et al., 2021; Cornacchia et al., 2022). A vortex forms in the vertical plane, determining a recirculation zone of finite length downstream of the patch (Folkard, 2005); in addition, a von Kármán vortex street occurs in the horizontal plane (Chen et al., 2013; Sukhodolova & Sukhodolov, 2012) but tends to disappear as the relative submergence increases.

An important aspect awaiting clarification is related to the role of the turbulent structures in the transport and exchange processes, especially in the transition between vegetated and non-vegetated areas where the effects of flow gradients and heterogeneities prevail (Folkard, 2011; Siniscalchi et al., 2012; Sukhodolov & Sukhodolova, 2006, 2010; Zong & Nepf, 2010). A heterogeneous distribution of vegetation on the bed creates abrupt roughness variations, which can lead to shear-induced vortices in both horizontal and vertical planes as well as to secondary circulations, with momentum exchange of comparable magnitude (Anderson et al., 2015; Vermaas et al., 2011).

Moreover, all the above-mentioned studies refer to straight channels, which are relatively rare in nature. More often, rivers exhibit curved or sinuous configurations, where nonlinear interactions between the curvature-induced cross-stream flow and the streamwise velocity distribution become as significant as the ratio R/B (R = local radius of curvature, B = channel width) decreases (e.g., Dietrich & Smith, 1983; Yalin, 1992; Blanckaert & Graf, 2001; Termini, 2015b; White et al., 2023, 2025), affecting hydrodynamics and sediment transport processes. The momentum transport by curvature-induced cross-stream flow motion plays a fundamental role in the downstream velocity and bed shear stress redistributions, especially in sharp bends (e.g., Blanckaert & Graf, 2001; Termini & Piraino, 2011).

Although several studies have been conducted to enhance our understanding of flow and turbulence characteristics in curved channels, the effect determined by the presence of aquatic vegetation is not still well known. Very few investigations exploring flow features in curved vegetated channels can be found in the literature. Zhang et al. (2013) numerically analyzed flow hydrodynamics in a bend partly covered by rigid vegetation and highlighted the formation of a large velocity gradient in the transition between the vegetated and non-vegetation zones. Termini (2016, 2017) examined flow characteristics and dispersion processes (Termini & Di Leonardo, 2018) in a high-curvature meandering bend with submerged herbaceous (flexible) vegetation uniformly distributed on the bed, verifying that vegetation strongly modifies the feedback between cross-stream flow and streamwise velocity (Termini, 2016, 2017) and the turbulent flow structure (Termini & Di Leonardo, 2018). Li et al. (2013) combined numerical model and experimental measures to analyze the effect of vegetation in the outer area of a 180°curved open channel, verifying that vegetation can protect the bank from erosion. Liu et al. (2016) experimentally investigated the effect of floodplain flexible artificial grass on the main flow pattern and conveyance capability of a small amplitude meandering compound channel. Yang et al. (2022) examined the influence of different emergent and rigid vegetation distributions on hydrodynamic characteristics in a 180° curved open channel. Other researchers focused on the effects of riparian vegetation on flow characteristics in the floodplain (White et al., 2023, 2025) and on the stabilization or metamorphosis of the meandering bends (Finotello et al., 2024; Ielpi et al., 2022).

To the authors' best knowledge, no experimental studies have been performed in curved channels partially covered by submerged flexible vegetation. Thus, despite its extensive presence in natural environments (see Figure 1, for example), little is known about the mechanisms that dominate mass and momentum exchange. The three-dimensional nature of flow in bends—especially in high-curvature ones—makes further complex the analysis of hydrodynamics and dispersion processes, particularly when influenced by heterogeneously distributed, flexible, and fully submerged vegetation. However, this knowledge is crucial for applications involving river morphodynamics and ecosystem evolution.

To contribute to addressing these knowledge gaps, the present study investigates flow patterns in a high-sinuosity meander bend with submerged, flexible vegetation patchily distributed. The analysis is conducted with the aid of data collected in a laboratory flume, designed to mimic the shape and characteristics of real high-sinuosity meanders (Da Silva et al., 2006; Parker et al., 1983; Yalin, 1992). Attention is restricted to the bend-apex area where curvature effects are significant. A key advantage of using a laboratory flume is the ability to control variables and to reproduce processes. This work complements previous studies (e.g., Termini, 2009; Termini & Di Leonardo, 2018; Termini & Piraino, 2011) conducted in the same flume, which examined the cases of absence of vegetation (i.e., isolating the channel's curvature effect) and uniformly distributed flexible vegetation (i.e., neglecting the impact of its heterogeneity). Their results demonstrated that vegetation can strongly alter the curvature-induced motion and the directionality of turbulent structures. This study extends these findings by investigating the effects of finite-size patches of submerged, flexible vegetation on flow. Thus, the specific aim of the present paper is to gain some insight into how the patchy vegetation configuration impacts: i) the curvature-induced flow pattern; ii) the turbulence characteristics and the dispersion and exchange processes.

FIGURE 1 Example of submerged patches of flexible vegetation along a bend of Bullin River (UK).

This paper is organized as follows. Section 2 describes the experimental apparatus and summarizes the results of previous works conducted in the same channel but with different bed conditions; the results are presented in section 3; discussion is reported in section 4 and, finally, concluding remarks in section 5.

2 | MATERIAL AND METHODS

2.1 | Experimental apparatus

Laboratory experiments were conducted in a recirculating flume, constructed at Department of Engineering - University of Palermo (Italy), of constant width $B = 0.50$ m and following the sine-generated curve, a shape that, as reported in previous literature works (e.g., Whiting & Dietrich, 1993; Da Silva et al., 2006; Termini, 2009; Termini & Piraino, 2011), effectively approximates real river meanders. The deflection angle at the inflection section was 110°, which is characteristic of a meander bend of high sinuosity (Parker et al., 1983; Yalin, 1992). At the apex section, the control parameter accounting for high-curvature effects, represented by the ratio R/B (Blanckaert, 2011), reaches a value of 1.94. This value falls within the range observed in natural rivers with sharp curvature (Hickin, 1977). The vertical side walls were made of 3 mm thick transparent plexiglass and 0.60 m height. The flow rate, measured through a Doppler instrument Mainstream EH 7000 (by Endress+Hauser s.r.l.), can be set through a valve allocated in the recirculating pipe and the water depth can be controlled through an adjusting weir at the downstream section of the flume. The bed, with longitudinal slope at the channel axis of 0.2%, was covered by aligned squared patches (length of patch's edge $L_P = 11.5$ cm; L_P/Li = ratio of patch size to interpatch distance = 1.15) of artificial grass-like flexible vegetation (see Figure 2), with a percentage of coverage of 10%. In order to consider realistic patch's characteristics, its aspect ratio $B_P/L_P = 1$ (with B_P = patch's width) was defined within the range (i.e., $0.18 < B_P/L_P < 1.25$) found for real species of flexible vegetation, as reported in the literature (e.g. *P. crispus*, *M. spicatum*,—see in Przyborowski et al., 2019; *G. densa*, *C. platycarpa*, *V.spiralis* – see in Cornacchia et al., 2022) and the patches' location corresponds to the minimum coverage value allowing an alternance of vegetated/non-vegetated areas promoting the species richness, as indicated by Looby et al. (2021). In the present work, analyses focus on the apex region of the central meander bend (Figure 2), which includes two aligned vegetated patches (P1 and P2 in Figure 2a-c). The run considered in the present work was conducted with flow discharge $Q = 0.124$ m^3/s (H = overall

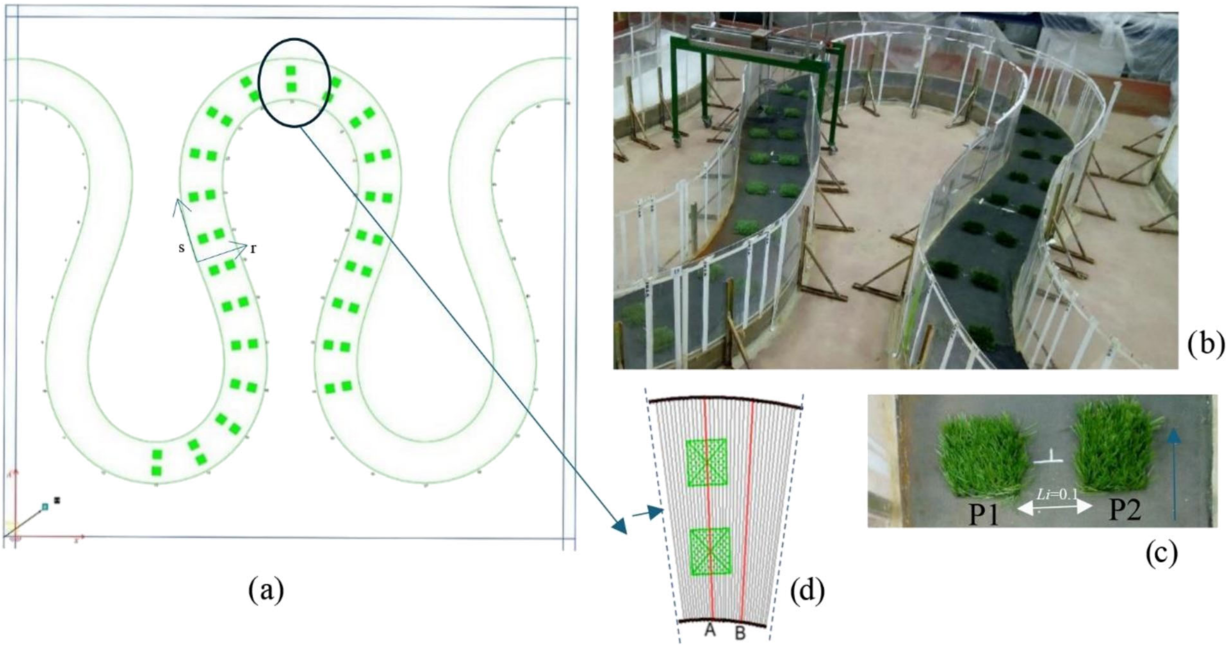

FIGURE 2 a) Plan view of the meandering flume with the local reference system; b) photo of the vegetated channel; c) particular of the two vegetated patches crossed by the apex section; d) measurement sections.

average water depth = 10.3 cm; $U = Q/[B \times H]$ = mean velocity = 0.24 m/s; $B/H = 4.8$, K_v = vegetation's undeflected height = 3.9 cm; k_v = bent height of the vegetated patch = 3.0 cm; H/k_v = overall average submergence = 3.43). This value of flow discharge was similar to values measured in natural rivers (e.g., Nikora et al., 2008) and used in previous works conducted both in the same flume as that of the present work (e.g. Termini, 2017; Termini & Di Leonardo, 2018) and in other laboratory flumes found in the literature (e.g., Blanckaert, 2011).

In natural rivers, width-to-depth ratio (B/H) varies greatly. However, it constitutes a crucial factor affecting streamwise and cross-sectional flow patterns (Whiting & Dietrich, 1993; Da Silva et al., 2006; Blanckaert, 2011). The B/H ratio considered in this work (B/H < 10) is characteristic of a narrow channel, where momentum transport by cross-sectional flow is significant—a behavior particularly important in sharp bends (Termini & Piraino, 2011).

During the experimental run, the instantaneous longitudinal, transversal and vertical flow velocities ($v_{s,t}$, $v_{r,t}$, $v_{v,t}$) were measured along 33 cross-sections, each spaced 9 mm apart, using a DOP 2000 (Signal Processing S.A.) with an accuracy of 0.09 cm/s and a sampling frequency of 2 MHz (Figure 2d). The first measurement section was half patch-width distant upstream to the entrance edge of the vegetated patches; the last measurement section was one patch-width distant from the exit edge of the patches for the longitudinal and vertical components and half patch-width for the transversal one. The width of the individual stems, d, was of 1.35 mm, the Reynolds number was $Re_d = Ud/\nu = 325$ (with ν = kinematic viscosity), and the porosity per unit bed area $\phi = V_f/V_t$ (V_f = fluid volume within the representative total volume and V_t = total volume) was 0.952. This value of porosity is comparable to that of most aquatic plants (Nepf, 2012; Nikora et al., 2013). Tension tests were conducted using a Zwick/Roell tension machine (maximum load cell of 5 kN and resolution of load force of 10^{-2}) to define the mechanical properties of the vegetation. These tests were performed until the stems, randomly selected within the patches, reached the breakage; the testing machine software ("textExpert II") in real time estimated the values of the stress σ_T and strain ε. Thus, by evaluating the Young modulus, E ($E = 1.33$ N/mm^2), and the horizontal second-order moments (i.e., $I_d = 4.1 \times 10^{-2}$ mm^4 $I_l = 9.0 \times 10^{-4}$ mm^4, with l = the stem's thickness), it was possible to estimate the stems' flexural rigidities $J_d = EI_d = 5.45 \times 10^{-2}$ Nmm^2, and $J_l = EI_l = 1.42 \times 10^{-3}$ Nmm^2. These values were comparable to those of the *Festuca arundinacea* (at the "young stage"), which is a species of monocotyledonous angiosperms belonging to the Poaceae family (or Gramineae), used in previous works (Termini, 2017; Termini & Di Leonardo, 2018). The Cauchy number, estimated according to the expression proposed by Whittaker et al. (2015) accounting for the possible reconfiguration of the flexible vegetation, was $Ca = \frac{\rho U^2 A_{p0} K_v^2}{EId} = 14.5$ (with A_{p0} = projected area in still air). This value of Ca is of same order of magnitude of real flexible vegetation ($5 < Ca < 100$) (Whittaker et al., 2015).

2.2 | Pertinent aspects and previous results obtained in the same channel

Before proceeding further, it is important to summarize here the key findings on the main flow and dispersion processes reported in previous studies conducted in the same meandering flume, and with almost equal flow discharge, both in the absence of vegetation and in the presence of submerged flexible vegetation uniformly distributed on the bed.

The experiments conducted without vegetation on the bed (e.g., isolating the curvature-induced flow pattern) indicated that:

i. as effect of the continuously changing curvature, the core of high streamwise velocities tends to shift along the meandering bend passing from the inner bank of the inflection section upstream to the outer bank of the inflection section downstream (Termini, 2009). At the apex section, the core of high streamwise velocities is found in the outer bank region, but at a certain distance from the bank because of the presence of a counter-rotating circulation cell (Termini & Piraino, 2011);

ii. the curvature-induced cross-sectional motion, considered composed of circulation and convective motions, varies along the bend, playing a significant role in redistributing streamwise velocity and bed shear stress (Termini and Piraino, 2011; Termini, 2015b). **At** the apex section, the convective motion prevails over the circulation motion in the inner-bank region, the main circulation cell occurs in the central region (i.e., for 0.25 < r/B < 0.75) and a counter-rotating circulation cell forms in the outer-bank region (i.e., for 0.75 < r/B < 1) near the free surface (Termini & Piraino, 2011);

iii. the turbulent kinetic energy assumes a peak value at about the eye of the above-mentioned circulation cells. At the apex section, high values of the lateral dispersion occur especially in the central area of the water depth of the central region. **In** outer-bank region, **the lateral dispersion assumes a slight peak just below the free surface** (Termini & Benistati, 2022).

The experiments conducted with uniformly distributed submerged flexible vegetation (e.g. neglecting the heterogeneity of vegetation) on the bed indicated that:

iv. the core of high streamwise velocity, which assumes values around one order of magnitude lower than that obtained in the absence of vegetation, also tends to move along the bend from the inner bank toward the outer bank but, contrary to what is observed in the absence of vegetation, it never reaches the outer region so that at the apex section the core of highest velocity is found in the central region. Consequently, the streamwise velocity assumes always low values near the outer bank (Termini, 2016, 2017).

v. the central-region curvature-induced circulation cell is suppressed, but small and thin circulation cells form at the top of the vegetated layer. Thus, the presence of the vegetated stems alters the directionality of turbulent structures that develop within and between the vegetated elements (Termini, 2016). The outer-bank counter-rotating cell also forms in the outer-bank region, but it is weaker and wider than that obtained in the absence of vegetation (Termini, 2017);

vi. the importance of the lateral dispersion significantly varies through the apex-section with the value of the relative submergence h/kv (with h = local water depth) **(Termini & Di Leonardo, 2018). Three behavioral regions** were identified **(Termini & Di Leonardo, 2018)**: **region 1** (h/k_v > 5), where the counter-rotating circulation cell inhibits the lateral dispersion; region 2 (**5 >** h/k_v > 2) where the lateral dispersion becomes important just over the top of vegetation; **region 3** (h/k_v < 2) where the lateral dispersion becomes more significant inside vegetation (Termini & Benistati, 2022; Termini & Di Leonardo, 2018).

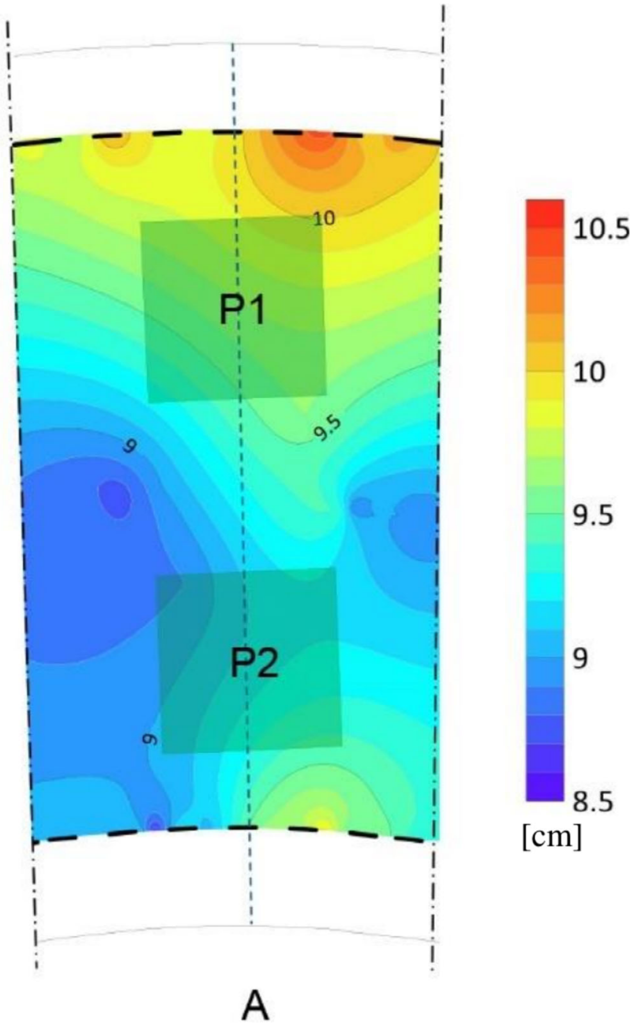

FIGURE 3 Contour map of the water depth, h, in the area including the vegetated patches.

3 | RESULTS

3.1 | Water depth and time-averaged velocity

As is well known, when flow enters a bend, the centrifugal force determines an outward flow pattern which causes water surface elevation at the outer bank. Cross-circulation is produced from the interaction of the forces associated with centrifugal acceleration, transverse water surface slope and bed shear stress (Chang, 1988; Whiting & Dietrich, 1993; Yalin, 1992). Along the bend, the water surface exhibits variable elevation so that, as the radius of curvature decreases from the bend entrance toward the apex, it increases near the outer bank and decreases near the inner bank. This causes the water surface slope to be steeper near the inner bank and flatter near the outer bank, resulting in a cross-stream surface slope at the apex section that tilts toward the inner bank (Termini, 2009).

On the contrary, the presence of vegetated patches at apex section A (Figure 3) results in a water depth that lacks the characteristic cross-stream slope toward the inner bank. The water depth is highest at the outer bank and shows a slightly decreasing trend moving toward the inner bank, but after reaching the channel axis, it increases again until it reaches the inner bank. This means that, because of the additional resistance due to the vegetated patches, similar values of patch-averaged water depth, h_a, and, consequently, similar values of the relative submergence h_a/kv, are obtained in the vegetated areas [i.e. h_a/kv = 3.3 and h_a/kv = 3.1 over patch P1 and P2, respectively - values within the range identifying the behavioral region 2 observed by Termini & Di Leonardo, 2018 in fully vegetated condition].

Contour maps of the time-averaged velocity components (streamwise, vertical, and transversal) are presented in Figure 4. These maps correspond to four horizontal planes located at relative water depths $z/H = 0.3$, 0.44, 0.61, and 0.81. Close to the top of vegetation (i.e., at $z/H = kv/H = 0.3$), the vegetated patches obstruct flow, decreasing velocity behind and—most significantly—downstream of them. Thus, in line with previous works in straight channels (e.g., Zong and Nepf, 2011) a wake zone is visible especially downstream of the patches. Above the vegetation, moving toward the free surface, all the velocity components increase in value. The streamwise component (Figure 4a), at $z/H = kv/H$, assumes negative low values around the patches, increasing gradually in value and changing the sign moving away from them. The extension of the region of reverse streamwise velocity is especially evident downstream of the patch P1.

A region of accelerated streamwise velocity is clearly visible in the centerline non-vegetated area, i.e. between the two patches. This indicates that the interpatch distance ($L_P/L_i = 1.15$) allows individual wakes to form behind the patches. This is consistent with Vandenbruwaene et al.' (2011) findings, analyzing interactions of vegetated patches growing in an initially bare landscape. They observed accelerated flow between the patches for interpatch distances greater than 0.43, until that the patches acted as a single unit as L_P/L_i exceeded approximately 6.67.

To better visualize the variation of the streamwise velocity in longitudinal direction, Figure 5 compares the profiles the patch-averaged streamwise velocity, [the symbol indicates the spatial average of time-average quantity; the spacing average has been applied in addition to the time average to limit the high level of heterogeneity], normalized by the mean velocity U, over the two patches (P1 and P2) and in the non-vegetated centerline area. Three zones can be distinguished in the longitudinal direction: zone 1 (at the left-hand side of the vegetated patches), zone 2 (in the patchy vegetated area), and zone 3 (at the right-hand side of the patchy vegetated area). In zone 1, the streamwise velocity is characterized by a decreasing trend of small negative values upstream of P1 and high positive values upstream of P2. On the contrary, in the centerline non-vegetated area, the streamwise velocity assumes increasing positive values, and this trend is also maintained in zone 2, that is, in the patchy vegetated area.

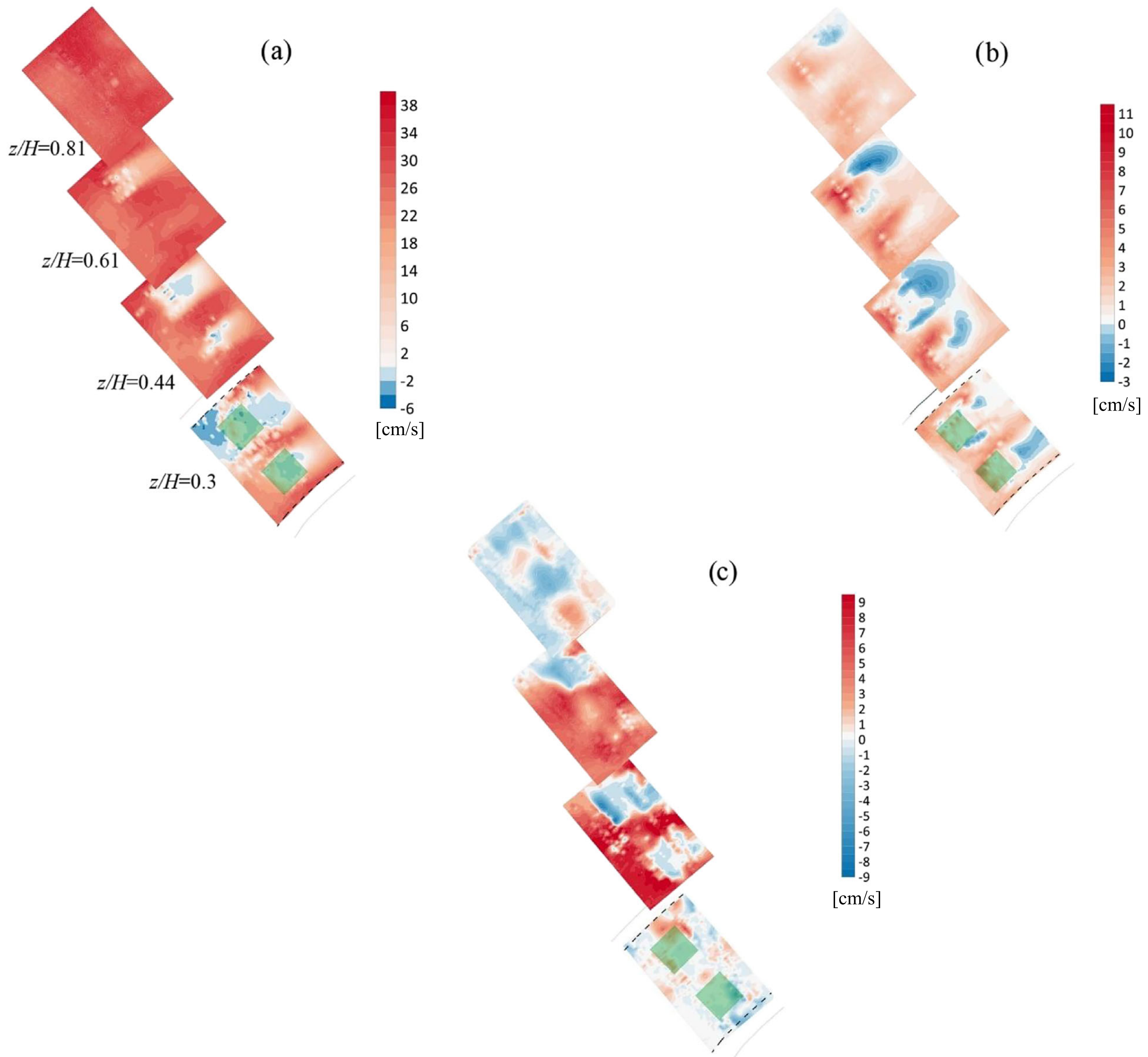

FIGURE 4 Contour maps of time-averaged velocity components: a) longitudinal component, v_s; b) vertical component, v_v; c) transversal component, v_r.

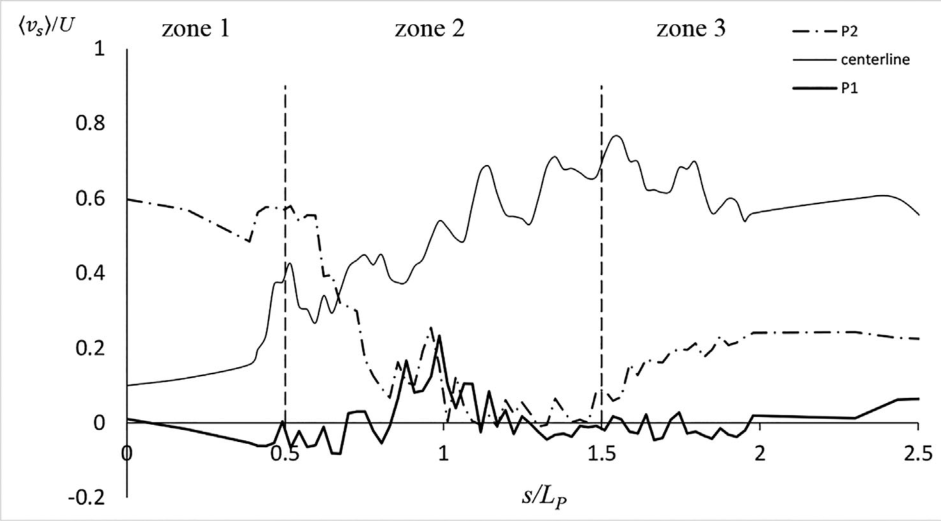

FIGURE 5 Longitudinal profiles of the normalized patch-averaged streamwise velocity, $\langle v_s \rangle / U$, (at $z/H = kv/H$) over the two patches (P1 and P2) and in the non-vegetated centerline area.

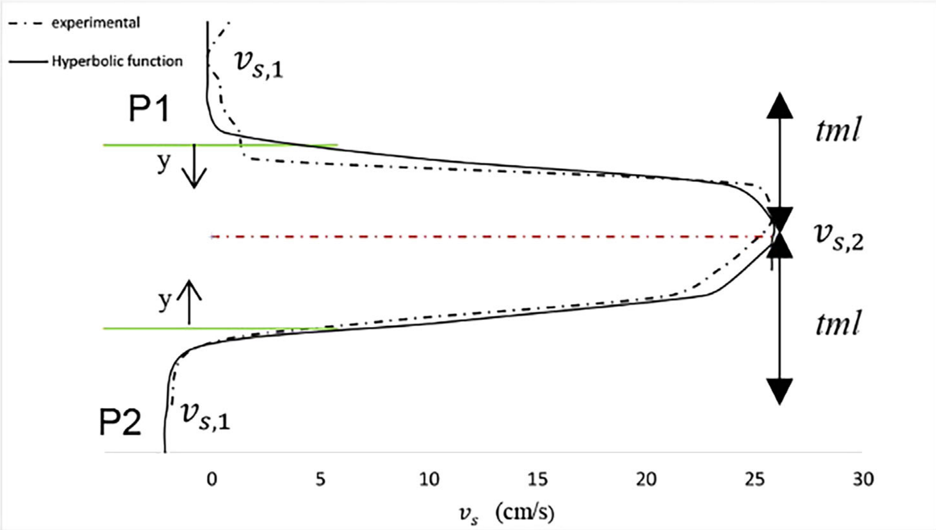

FIGURE 6 Transversal profiles of v_s at $z/H = kv/H$ in the interpatch area of the apex section A.

Here (zone 2), within each patch, the streamwise velocity first increases to a positive peak approximately at the center of the patch, then decreases again. In zone 3, the streamwise velocity exhibits different patterns depending on the location: downstream of patch P1, the streamwise velocity assumes small negative values in a region extending for approximately *0.8Lp*, after which it starts to increase; downstream of patch P2, the streamwise velocity maintains small positive values for a length extending around *0.25Lp*, with an increasing trend until reaching a value greater than that downstream of patch P1. In the centerline, the streamwise velocity assumes a slightly decreasing trend. Thus, Figure 5 indicates that the wake zone forming directly downstream of the vegetated patch extends for a length that increases as the local channel's curvature increases, that is, passing from patch P2 (near the inner bank) to patch P1 (near the outer bank).

Figures 4 and 5 also illustrate the effect determined by the presence of the vegetated patches on the flow velocity pattern. In contrast to what is observed in the absence of vegetation—where the core of high streamwise velocities was found near the outer bank of the apex section (e.g., Termini, 2009; Whiting & Dietrich, 1993)—in these figures, the core of high positive streamwise velocities shifts toward the inner bank, while small negative values are found near the outer bank.

To analyze the variation of the streamwise velocity in the patch-adjacent lateral area, Figure 6 reports the profiles of the streamwise velocity along the apex section A, which crosses the center of the vegetated patches. A clear positive velocity gradient is observed close to the lateral edge of each vegetated patch: the streamwise velocity suddenly increases moving away from the patch and the experimental profile, which extends from the lateral patch's edge toward the channel's axis, shows a changing concavity, with the formation of an inflection point before reaching its maximum velocity at the axis. A lateral shear layer forms close to each vegetated patch. In line with previous works on vegetated channels (e.g., Ghisalberti & Nepft, 2002; Carollo et al., 2008), the presence of the inflection point suggests a mixing layer scheme, so that the velocity profile can be considered composed of two layers of constant velocity separated by an intermediate mixing layer containing the inflection point. Accordingly, the experimental profile extending from the lateral patch's edge toward the channel's axis (Figure 6) has been considered composed of two layers characterized by the lowest, $v_{s,1}$, and the highest,$v_{s,2}$, velocity values, respectively, and the intermediate mixing layer. The spatial extent of the lateral shear layer has been defined by the thickness of the mixing layer. The hyperbolic tangent function (e.g., Ghisalberti & Nepft, 2002; Carollo et al., 2008) has been used to fit the experimental profile as:

$$v_s = \overline{v_s} + \frac{\Delta v_s}{2} tanh\left(\frac{y-\bar{y}}{2\theta}\right) \tag{1}$$

with

$$\theta = \int_{-\infty}^{+\infty}\left[\frac{1}{4} - \left(\frac{v_s - \overline{v_s}}{\Delta v_s}\right)^2\right]dy \tag{2}$$

where y is the generic transversal distance from the lateral patch's edge (Figure 6), $\overline{v_s} = (v_{s,1} + v_{s,2})/2$, $\bar{y}$ is the distance from the bed where $v_s = \overline{v_s}$ and $\Delta v_s = v_{s,2} - v_{s,1}$; θ is the momentum thickness (Ghisalberti & Nepf, 2002) which also quantifies the reduced momentum flux determined by the vegetation drag.

Thus, the mixing layer thickness has been defined as the transverse distance between the points where $v_s = v_{s,1}$ and $v_s = v_{s,2}$, measured from the lateral patch edge. Based on this definition, the shear layer extent was approximately *0.76Lp* near patch P1 and *0.92Lp* near patch P2. This indicates that the shear layer slightly increases as the local radius of curvature decreases. Shear-induced vortices form in the horizontal plane close to the lateral edge of each patch, driving momentum exchange in the central area of the channel. The value of momentum thickness θ was around *0.04Lp*, indicating the vegetation drag action in the lateral patch-adjacent area.

Reduced vertical velocity values (Figure 4b) are also observed downstream of the patches, at $z/H = kv/H = 0.3$, with negative values occurring in the wake zone, especially downstream of patch P2. Moving from the bed toward the free surface, the region of negative vertical velocity becomes more pronounced downstream of patch P1, gradually diminishing in extent. The transversal velocity (Figure 4c), at $z/H = kv/H = 0.3$, shows alternating small positive and negative values behind and downstream of the patches. Moving upward from the bed toward the free surface, negative transverse velocity regions appear near the two patches, decreasing in extent toward the free surface. Thus, while confined areas of negative transversal and vertical velocity components form downstream of the vegetated patches, positive values persist in the lateral area between the patches. This suggests the formation of complex three-dimensional flow structures around and downstream of the vegetated patches, which influence not only the streamwise velocity distribution but also the cross-sectional flow pattern.

To better visualize this influence, Figure 7 shows the contour maps of the streamwise velocity and the cross-sectional velocity ($v_t = \sqrt{v_r^2 + v_v^2}$), in the apex section A and in section B, which is located approximately at half patch-width downstream from the exit edge of the patches. Figure 7b also reports the vectorial distribution of v_t. In section A, the streamwise velocity (Figure 7a) assumes small values close to the bed, decreasing and changing the sign around the top of the vegetated layer, where evident regions of negative velocity values form, especially over patch P1. The cross-sectional velocity distribution (Figure 7b) indicates that: i) the typical curvature-induced central-region circulation cell—observed in absence of vegetation by Termini and Piraino (2011)—appears to be divided into two smaller circulation cells developing in the central area of the water depth and a counter-rotating circulation motion also tends to form in the outer bank region; ii) circulation cells of size proportional to the vegetated stem's width form at the top of the vegetated layer; iii) additional circulation cells appears at the lateral edges of the patches. In section B, the distribution of the streamwise velocity (Figure 7a) is similar to that observed in section A, but the regions of negative values—which also occur in this section around the level *kv/h*—correspond to thinner fluid areas. Two curvature-induced circulation cells also form downstream of the vegetated patches (Figure 7b), but they are larger than those in section A. Additionally, a counter-rotating circulation motion tends to develop in the outer-bank region, encompassing a smaller fluid area than in section A. Thus, from Figure 7, it is clear that, because of the heterogeneous distribution of vegetation, velocity gradients are generated near the lateral edges of the patches, and shear-generated circulation cells are produced beyond the stem-generated cells.

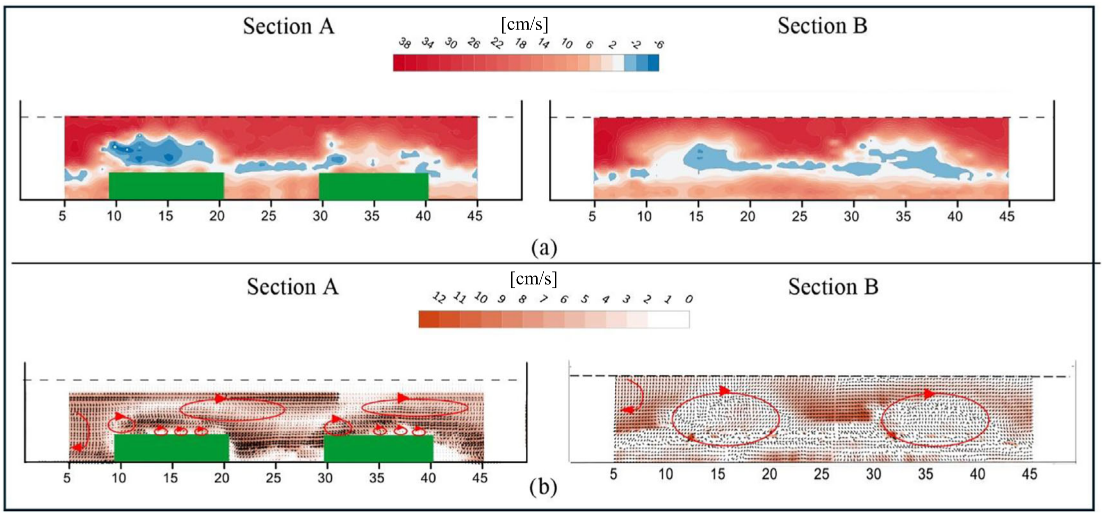

FIGURE 7 a) Contour map of the streamwise velocity in sections A and B; b) contour map and vectorial distribution of the cross-sectional velocity $v_t = \sqrt{v_r^2 + v_v^2}$ in sections A and B.

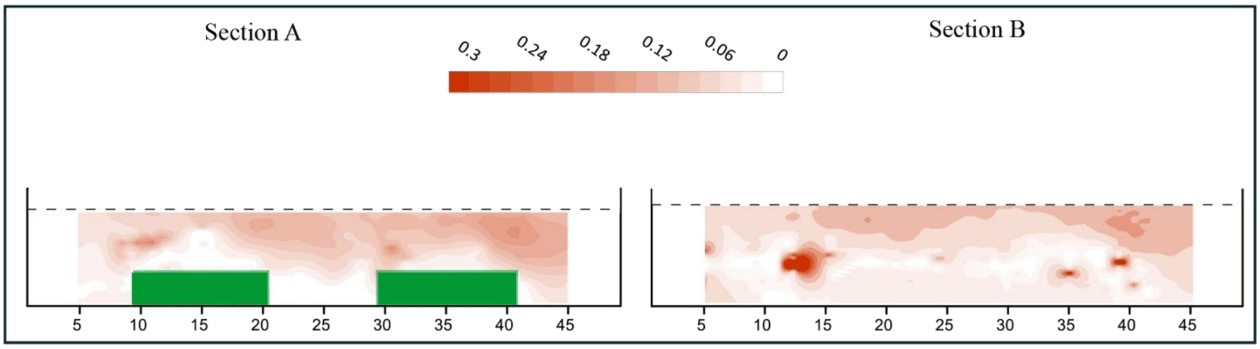

FIGURE 8 Contour maps of the normalized turbulent kinetic energy $k'/(U^2/2)$

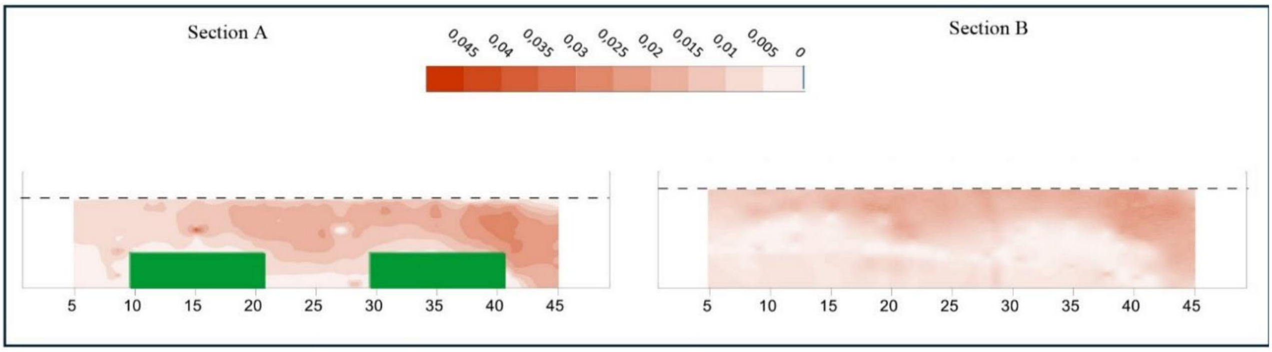

FIGURE 9 Contour maps of the normalized turbulent shear stress $-\overline{v_s' v_z'}/U^2$.

3.2 | Turbulent kinetic energy and Reynolds stress

The energy associated with turbulence is analyzed by the turbulent kinetic energy per unit of mass $k' = \frac{\overline{v_s'(t)^2} + \overline{v_r'(t)^2} + \overline{v_z'(t)^2}}{2}$ (with v_s', v_r', v_z' = turbulent velocity components in longitudinal, transversal and vertical directions). Figure 8 reports the contour maps of k', normalized by $U^2/2$, in sections A and B.

In section A, localized high peaks of $k'/(U^2/2)$ are obtained over the vegetated patches near their lateral edge, in the transition between the non-vegetated and the vegetated areas. Two regions of high values of $k'/(U^2/2)$ are also observed in the central area of the water depth with a peak at about the eye of the two curvature-induced circulation cells shown in Figure 4b. These regions can also be observed in section B, where localized high peaks of $k'/(U^2/2)$ occur approximately at the water level corresponding to the top of vegetation. Thus, Figure 8 suggests that in section A, shear-generated turbulent kinetic energy prevails over that from cross-sectional circulation, while this behavior is not as pronounced in section B.

The streamwise turbulent flux in sections A and B can be analyzed from the distribution of turbulent shear stress $\tau_{sz}/\rho = -\overline{v_s' v_z'}$, normalized by U^2 (Figure 9). In section A, high values of normalized turbulent shear stress occur in the central area of the water depth, in the correspondence of the two curvature-induced small circulation cells; small peaks occur especially over the vegetated patch P1 and close to the lateral edge of the patch.

In section B, lower values of normalized turbulent shear stress are found downstream of the patches. Furthermore, localized low peaks are present at the water level corresponding to the top of vegetation, providing additional evidence of the vegetation's influence. Figure 9 confirms that the patchy vegetation configuration influences the turbulent momentum transfer in the bend-apex area. In section A, the stem-generated and the shear-generated turbulent momentum transfer prevail over that related to the curvature-induced cells. In section B—that is, downstream of the patchy area—this last effect becomes again more significant, although the influence of stem oscillations persists so that localized low-magnitude peaks τ_{sz}/ρ occur around the water level corresponding to the top of the vegetation. Thus, vegetation acts as a source of turbulence and momentum transfer also in the patch-adjacent area.

3.3 | Lateral dispersion

The influence of the vegetated patches on the lateral dispersion has been investigated through the transversal dispersion coefficient, K_{rr}. According with previous works on vegetated flows (Nepf, 2012; Nepf & Vivoni, 2000; Tanino & Nepf, 2008), K_{rr} has been defined as a function of the product of the root square of the turbulent kinetic energy, $\sqrt{k'}$, representing the velocity scale, and the average stem's blade width, d, representing the average turbulent length associated with mixing due to turbulent eddies. The spatial-averaged transversal dispersion coefficient, $\langle K_{rr} \rangle$, has been also estimated, by averaging the time-averaged values along the same elevation over three measurements verticals, as: $\langle K_{rr} \rangle = \left\langle \sqrt{k'} \right\rangle d$.

The vertical profiles of the normalized local and spatial-averaged lateral dispersion coefficients, $K_{rr,n}, \langle K_{rr,n} \rangle = \frac{\sqrt{k'}d}{Ud}, \left\langle \frac{\sqrt{k'}d}{Ud} \right\rangle = \frac{\sqrt{k'}}{U}, \left\langle \frac{\sqrt{k'}}{U} \right\rangle$, in five representative locations (L1-L5) of sections A and B are reported in Figure 10. In section A, within the patches (i.e., locations L2 and L4), $\langle K_{rr,n} \rangle$ assumes small values inside the vegetated layer, with a

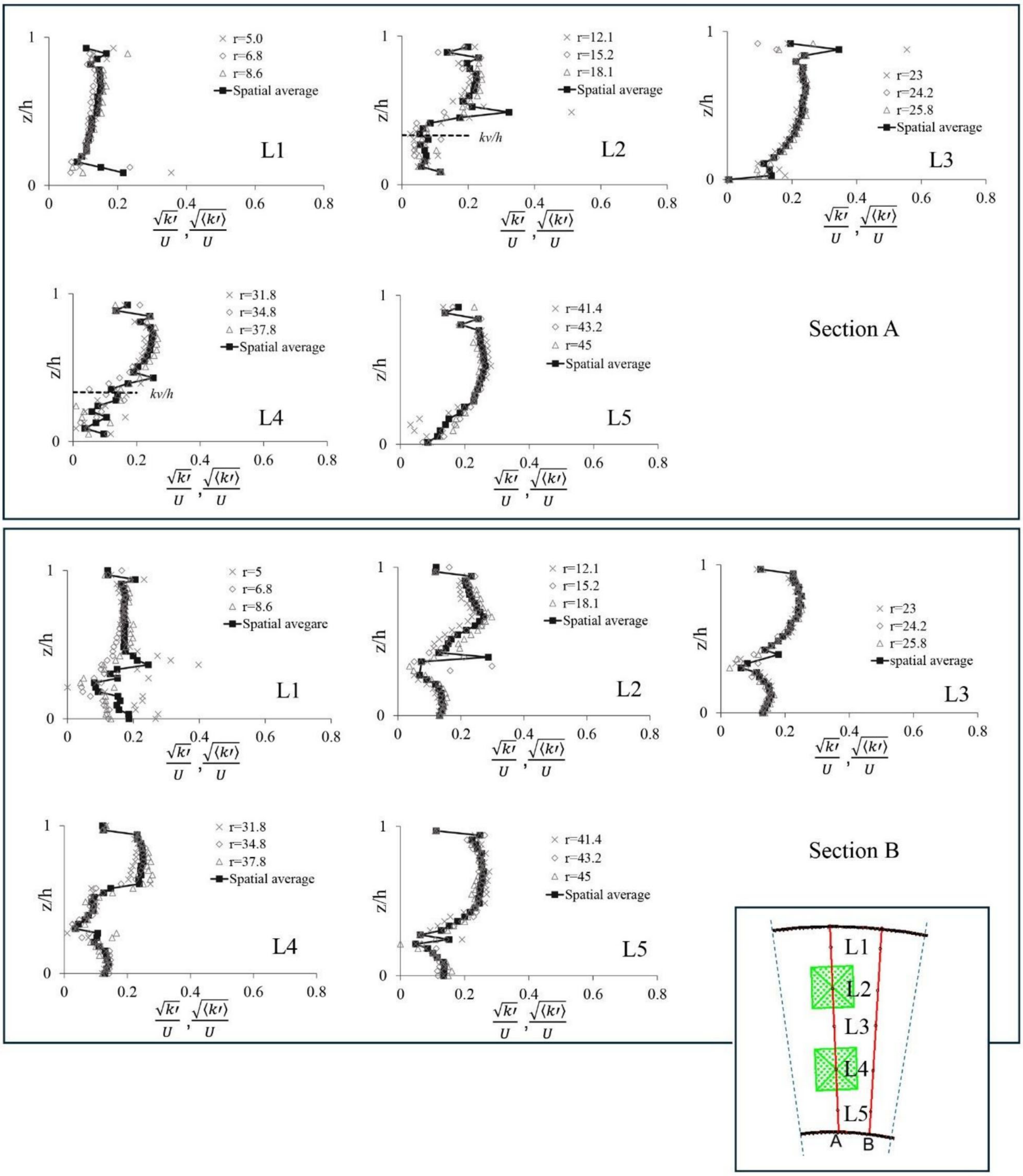

FIGURE 10 Local and spatial-averaged normalized lateral dispersion coefficient, $K_{rr,n} = \frac{\sqrt{k'}}{U}$, $\langle K_{rr,n} \rangle = \left\langle \frac{\sqrt{k'}}{U.} \right\rangle$

peak close to the vegetation top, then an increasing trend can be observed moving toward the free surface, with a slight decrease close to the free surface. In non-vegetated areas (i.e., locations L1, L3, L5), $\langle K_{rr,n} \rangle$ shows an increasing trend passing from the bed to the free surface, with a slight peak value just below the free surface. This increasing trend is especially evident in L3 and L5 (i.e., in the centerline and in the inner bank region), being less evident in the outer-bank region (location L1) because of the adjunctive effect of the counter-rotating circulation motion developing in this region. This is consistent with what observed in the outer-bank region of the same channel in the absence of vegetation on the bed (Termini & Benistati, 2022). In section B, the vertical profiles of $\langle K_{rr,n} \rangle$ exhibit a trend similar to those in non-vegetated areas of section A at all considered locations. However, a discontinuity—particularly pronounced in profiles L2 and L4—appears around the water level corresponding to *kv/h*.

Thus, Figure 10 indicates that, in line with what observed in fully vegetated channel (Termini & Di Leonardo, 2018), within the vegetated patches the lateral dispersion plays an important role just over the top of vegetation; in the lateral patch-adjacent areas the lateral dispersion is more significant in the central part of the water depth, a behavior consistent to that observed in the same channel in the

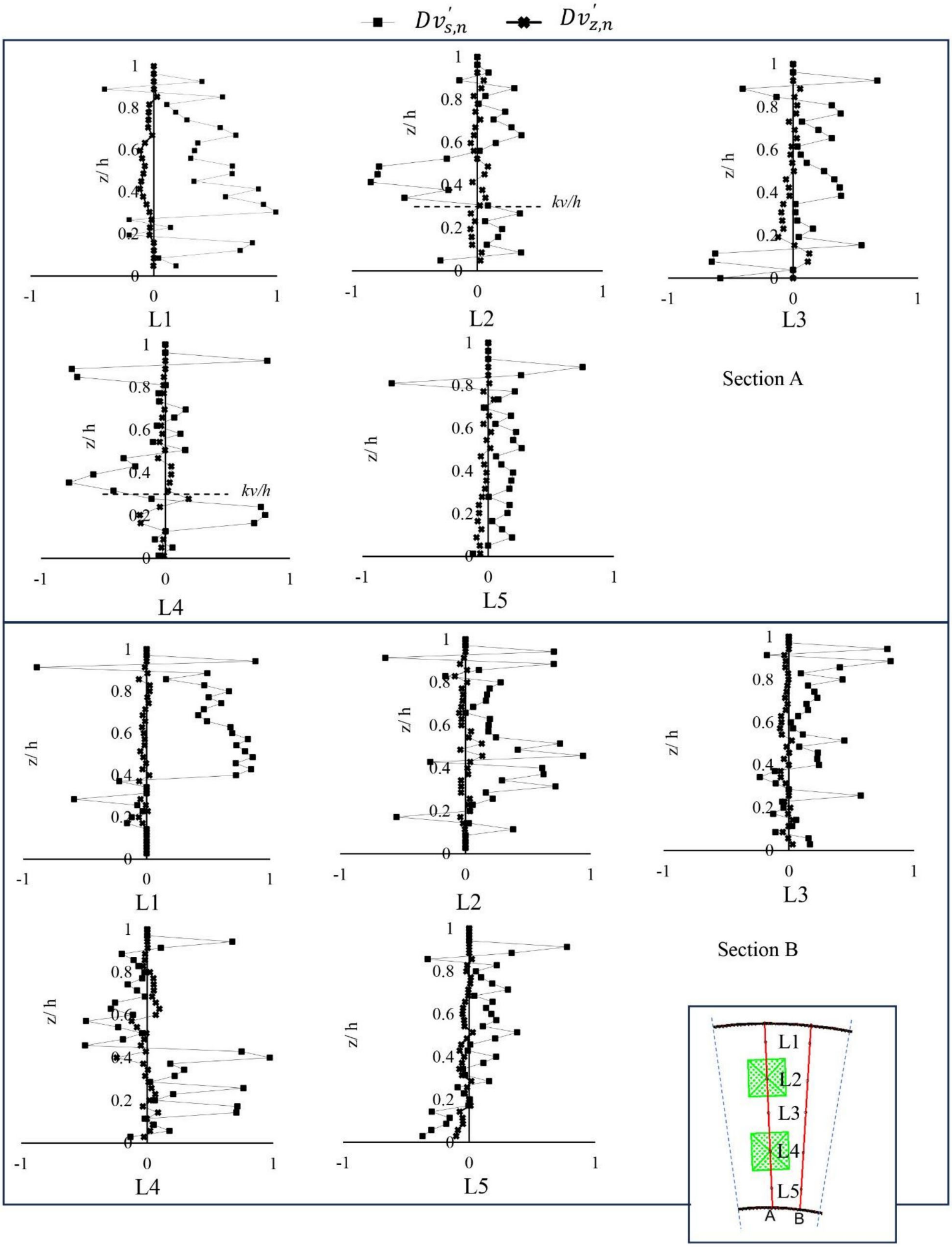

FIGURE 11 Profiles of $Dv'_{s,n}$ and Dv'_{zn} in the selected locations

absence of vegetation (Termini & Benistati, 2022). This last trend has been also observed downstream of the patchy-vegetated area (section B), although a discontinuity in the $\langle K_{rr,n} \rangle$ profiles occurs at the level corresponding to the top of vegetation, indicating still the influence of vegetation in the wake zone.

3.4 | Higher order moments and vertical and streamwise turbulent diffusion

Higher order moments, $Dv'_{s,n} = \overline{v'_s(t)^3} / \overline{v'_s(t)^2}^{3/2}$ and $Dv'_{z,n} = \overline{v'_s(t)^2 v'_z(t)} / \overline{v'_s(t) v'_z(t)}^{3/2}$, have been estimated to investigate the streamwise transport of turbulent kinetic energy and the turbulent diffusion in the vertical direction, respectively.

Figure 11 reports the profiles of $Dv'_{s,n}$ and $Dv'_{z,n}$ in the locations L1÷L5 of sections A and B. $Dv'_{s,n}$ and Dv'_{zn} have generally opposite peaks at the same relative depth, with $Dv'_{s,n}$ always larger than $Dv'_{z,n}$. In section A, within the vegetated patches (i.e., locations L2 and L4), large negative values of $Dv'_{s,n}$ and small positive values of $Dv'_{z,n}$ are found just above the vegetation, while the opposite behavior is observed inside it. This indicates slow fluid motion upward from the patch (i.e., ejection-like motion) and the formation of coherent vortices close to the vegetation. In locations without vegetation (i.e., locations L1, L3 and L5), $Dv'_{s,n}$ is generally positive and $Dv'_{z,n}$ negative. This trend indicates a streamwise fluid motion downwards due to reverse flow. Notably, the highest values of $Dv'_{s,n}$ are found near the outer bank (i.e. in L1). However, this pattern is accompanied by a discontinuity at the relative depth kv/h, which is particularly pronounced in L3 and L5. In section B, $Dv'_{s,n}$ and $Dv'_{z,n}$ generally tend to assume a behavior similar to that obtained in section A in the locations (L1, L3, L5) without vegetation. However, in L2 and in L4 alternating peaks of opposite sign for $Dv'_{s,n}$ and $Dv'_{z,n}$ is observed at the relative depth level corresponding to kv/h, indicating the influence determined by the vegetated stems oscillation in the wake zone.

4 | DISCUSSION

The analyses presented in this work provide a description of the effects of the patchy distribution of submerged flexible vegetation on flow pattern and dispersion processes in the apex area of a meandering bend.

Results principally highlight that the presence of patchy vegetation distribution determines a complex three-dimensional flow structure and alters the curvature-induced flow velocity pattern typically observed in sharp river bends (Blanckaert, 2010; Chang, 1988; Termini, 2009; Whiting & Dietrich, 1993; Yalin, 1992). The additional resistance offered by the patchy distribution of vegetation along the bend limits the outward flow pattern at the bend entrance and, consequently, the superelevation at the outer bank. This determines at the apex section almost equal values of the water depth over the patches and, therefore, almost equal values of the relative submergence. Consequently, in the bend-apex area, the water surface does not exhibit the typical cross-stream slope tilting toward the inner bank—a feature observed both in the absence of vegetation (Termini, 2009) and in the presence of uniformly distributed vegetation (Termini & Di Leonardo, 2018) —and the streamwise water surface slope ($\partial h/\partial s$) assumes the same sign close to the banks, being positive until the exit edge of the patches and then becoming negative.

Furthermore, because of the additional drag force exerted by the vegetated elements, wake regions of reduced velocities form not only within but also behind the vegetated patches. According to literature studies (Bouma et al., 2007; Schoelynck et al., 2012; Schulz et al., 2003), this region of reduced velocities could promote sediment deposition around the vegetated patches.

Negative low values of the streamwise and vertical velocity components occur in the wake zone, indicating the presence of a reverse flow on the vertical plane determined by the stems' oscillation. The vertical reverse flow zone extends downstream of the exit edge of the vegetated patches. Although this is line with previous studies conducted in straight flumes with submerged finite vegetated patches (e.g., Siniscalchi et al., 2012; Li et al., 2014; Devi & Kumar, 2016; Liu et al., 2018; Kazem et al., 2021; Cornacchia et al., 2022), in the examined case the extent of this region is not equal for the two patches but it varies with the local channel's curvature—extending slightly less than one patch-width downstream of the patch closer to the outer bank (P1) and approximately a quarter patch-width downstream of the patch closer to the inner bank (P2). The difference in extension may be also attributed to the closer spacing of vegetated patches in the longitudinal direction as the radius of curvature decreases passing from the outer to the inner bank. The presence of a region of accelerated streamwise velocity between the two patches confirms that a distinct wake zone is generated for each vegetated patch, a behavior consistent with the so-called wake interference flow regime observed in patchy vegetated straight channels (e.g., Vandenbruwaene et al., 2011; Zhang & Nepf, 2025).

In fact, the abrupt variation in bed roughness results in a significant streamwise velocity gradient in the patch-adjacent lateral area. A shear layer forms close to the lateral edge of each vegetated patch, with the development of shear-induced vortices that drive momentum exchange in the central area of the channel.

The transversal velocity shows at the top of vegetation an alternance of positive/negative low values over and downstream of the vegetated patches, indicating the formation of very small turbulent structures. But, moving from the bed toward the free surface, larger confined areas of negative transversal and vertical velocities are found downstream of the vegetated patches while positive values are maintained in non-vegetated areas between the two patches, indicating the development of larger three-dimensional flow structures which could exert an important role in the sediment and mass distribution along the vertical direction (Przyborowski & Łoboda, 2021; Biggs et al., 2019). This behavior agrees with other literature studies (Chang & Constantinescu, 2015; Liu et al., 2008; Liu et al., 2018) highlighting that the interaction of the small vortices forming over the vegetated patches tends to merge a larger turbulent structure around the edge of the patch.

The analysis of cross-sectional flow in the apex section A revealed the formation of three key features: i) shear-generated vortices at the lateral interface of the patches; ii) stem-generated vortices at the top of the vegetation; iii) two curvature-induced circulation cells in the central part of the water depth.

This further confirms that the presence of the two vegetated patches on the bed alters the curvature-induced circulation motion typically seen in the bend-apex area of meandering bends (Termini & Piraino, 2011). In particular, the central-region curvature-induced circulation cell, observed at the apex section in the absence of vegetation on the bed (Termini & Piraino, 2011), is thereby split into two smaller circulation cells that enlarge as they propagate into the downstream non-vegetated area. We hypothesize that in the absence of vegetation in the entire channel reach downstream, these cells would eventually merge to re-form a single, dominant circulation cell in the central region. In contrast, findings reported by Termini (2017, 2018) for the same bend-apex area indicate that the presence of vegetation uniformly distributed on the bed would suppress the central-region curvature-induced circulation cell, resulting in only stem-generated vortices developing at the top of the vegetated layer.

Thus, the comparison of the cross-sectional flow pattern over vegetated patches (present work) with those over uniformly distributed bed vegetation (Termini, 2017, 2018) and over unvegetated conditions (Termini & Piraino, 2011) suggests that the presence of submerged flexible vegetation islands in natural river bends may modify the typical curvature-induced motion through three primary mechanisms: i) fragmentation of the main central-region curvature-induced circulation cell into smaller cells, which decrease in size as vegetation cover increases until being completely suppressed under uniform vegetation cover; ii) generation of stem-scale vortices above the vegetated layer; iii) development of shear-generated vortices at the vegetated-non-vegetated interface regions. This result aligns with the findings of Sukhodolov & Sukhodolova (2010) in a lowland river, which demonstrated that vegetation islands transform the flow structure over a non-vegetated riverbed, creating a highly fragmented, complex flow pattern spatially arranged according to the distribution of patches.

The fragmentation of the flow pattern modifies the feedback between the momentum transport by cross circulation and the streamwise velocity distribution. Unlike previous observations without vegetation (Termini, 2009) or with uniform vegetation (Termini & Di Leonardo, 2018) at the bend-apex area, the present case shows at the apex section two high-velocity cores in the central water depth and accelerated flow between the two patches.

Based on the above-mentioned results, it can be summarized that the presence of the vegetated islands in meandering river bends could limit the erosive action of flow and, hereby, the sediments movement from the outer to the inner regions.

Results also indicate that the interfacial region of the patch is the region of highest shear and turbulent kinetic energy. This agrees with findings obtained from Zhang et al. (2013) in a curved channel partly covered by rigid vegetation. The turbulent kinetic energy exhibits localized peaks near the lateral patch's edges and alternating high-low values elsewhere in the patches. The distribution of the turbulent shear stress τ_{sz} confirms the presence of regions of shear especially close to the lateral patch's edge. The positive streamwise velocity gradient (Figures 4 and 6) and increase of shear stress (Figure 9) indicate a positive shear production in the lateral patch-adjacent area. This is associated with the increased lateral flow and momentum exchange in the transition between the vegetated and the non-vegetated areas. Over the patches, localized peaks of τ_{sz} occur, in agreement with what is observed in fully vegetated configuration (Termini & Di Leonardo, 2018). Additionally, high values of the turbulent kinetic energy occur approximately near the centers of the two curvature-induced circulation cells. This behavior differs from that observed in the apex section in vegetation-free conditions, where turbulent kinetic energy typically peaks at the eye of the central-region circulation cell (Blanckaert, 2010; Termini & Piraino, 2011). Instead, in the present case, the effects of stem-generated and shear-generated turbulence appear more significant than those from curvature-induced circulation cells. Conversely, in section B—that is, in the non-vegetated area downstream of the patches—the influence of curvature-induced cells once again becomes dominant.

The lateral dispersion and vertical exchange assume a different trend inside and outside of the vegetated areas. While within the vegetated patches, the lateral dispersion plays an important role just over the top of the vegetation, outside of the vegetated areas, the lateral dispersion increases passing from the bed toward the free surface, assuming an important role in the central region of the water depth. However, a discontinuity in the vertical profiles of $\langle \boldsymbol{K}_{rr,n} \rangle$ has been observed at the water level corresponding to the top of the vegetated layer, confirming the influence of stem fluctuations on the dispersion process, even in the transition between vegetated and non-vegetated areas. In the outer-bank (non-vegetated) area, because of the adjunctive effect of a counter-rotating circulation motion, the lateral dispersion assumes small values almost uniformly along the water depth. On the contrary, the turbulent diffusion in the vertical direction, $\boldsymbol{Dv'_{s,n}}$, is more significant. This is consistent with what was observed in the same channel in the absence of vegetation on the bed (Termini & Benistati, 2022). Within the vegetated patches, a strong coherent turbulent activity occurs just close to the top of vegetation, with high-speed fluid movement toward the free surface ($\boldsymbol{Dv'_{s,n}} < 0$, $\boldsymbol{Dv'_{z,n}} > 0$) above the vegetation and high-speed fluid movement toward the bed ($\boldsymbol{Dv'_{s,n}} > 0$, $\boldsymbol{Dv'_{z,n}} < 0$) below the vegetation. This highlights the formation of coherent turbulent structures close to the vegetated layer, confirming that the vegetation is a sink of turbulent motion (Nezu and Sonjau, 2008; Tinoco and Coco, 2016; Termini & Di Leonardo, 2018). The stem-scale vortices, generated on the vertical plane by the shear flow at the top of the vegetation, determines vertical mixing across the upper- and within-vegetation layers. In the non-vegetated areas, the streamwise momentum transport prevails, but with a discontinuity at the level corresponding to kv/h. This behavior, which is also observed downstream of the vegetated patches (section B), further confirms the influence determined by the vegetated stems oscillation also in the non-vegetated areas.

5 | CONCLUDING REMARKS

In the present work, the flow characteristics in the bend-apex area of a high-sinuosity meandering flume with squared patches of fully submerged flexible on bed have been investigated to give insights applicable to river management and ecological restoration.

The obtained results demonstrated that the presence of the vegetated patches alters the flow pattern in the bend-apex area, modifying the curvature-induced circulation motion and the feedback between it and the streamwise velocity. The main curvature-induced circulation cell is divided into two smaller circulation cells, limiting its erosion action, and two cores of high streamwise velocity have been found in the central part of the water depth. Stem-scale vortices generate above the vegetated layer, and shear-generated vortices develop at the vegetated-non-vegetated interface regions. Here, accelerated streamwise flow velocities are clearly visible.

A wake zone of reduced velocity forms downstream of the exit edge of the vegetated patches. This is consistent with previous findings obtained in straight channels (e.g., Schoelynck et al., 2012; Schulz et al., 2003; Siniscalchi et al., 2012), but in the present case, the extension of this region is not constant along the bend, but it depends on the local channel's curvature.

The interfacial region between the vegetated and the non-vegetated areas is the region of the highest shear and turbulent kinetic energy. Regions of alternating high-low values of turbulent kinetic energy form over the patches.

The lateral dispersion and the mass exchanges are strongly influenced by the presence of the vegetated patches and by the turbulent structures which form between the vegetated and the non-vegetated areas. In particular, the presence of flexible vegetation determines a reduction of the size of the turbulent structures and limits the transport process in the vegetated areas, but it also exerts an influence in the transition toward the non-vegetated ones. In the vegetated areas, the lateral dispersion plays an important role just over the top of vegetation, where stem-scale vortices occur. A strong coherent turbulent activity occurs just below the top of vegetation with high-speed fluid movement toward the free surface, which could lead to resuspension of sediments. In the transition from the non-vegetated to the vegetated areas, the lateral dispersion is more significant in the central region of the water depth, although a low peak occurs at *kv/h*, indicating the effect determined by shear-generated vortices. The interaction of these eddies influences flow velocity in the downstream region, having an important role in the mass exchange in the central area of the channel and in the vertical direction.

In summary, the presence of submerged vegetated islands in natural river bends modifies the typical curvature-induced circulation motion and streamwise velocity distribution, determining a fragmented flow pattern according to the patches' configuration. Bearing in mind that in the examined two-patches case the main central-region is divided into two smaller curvature-induced circulation cells, it is expected that the size of these cells decreases as the patches mosaic covering increases, until being suppressed in fully vegetated beds. Consequently, the presence of vegetated islands in natural bends could limit the erosive action of cross-circulation along the bend, and this limiting effect increases with the amount of the vegetation cover. Results also indicate that the patchy vegetation configuration exerts a peculiar role on ecosystem functioning in natural bends. A region of reduced velocity, which could serve as a shelter for different species, forms downstream of the vegetated patches, but its extent varies along the bend depending on the local radius of curvature. Moreover, peculiar flow-vegetation interaction mechanisms occur in the lateral interfacial regions. Here, the influence of oscillating vegetated stems is still evident, generating high turbulent kinetic energy and enhancing lateral dispersion at the water level corresponding to the top of the vegetation.

It should be noted that, although this work has provided insight into the effect of flexible, submerged vegetated patches on main flow patterns and exchange processes in the apex-bend area, further work is also being addressed to extend it by investigating the turbulence structure in detail and modeling the variation of the drag coefficient, caused by the shear structure developing around the patches, and vegetation reconfiguration. The results, along with a detailed term-by-term analysis of the governing equations, will be discussed in a subsequent report.

ACKNOWLEDGEMENTS

This study was conducted partially with financial support of Project "National Biodiversity Future Center - 643 NBFC" CUP B73C22000790001, under the National Recovery and Resilience Plan (NRRP), 644 Mission 4 Component 2 Investment 1.4 - Call for tender No. 3138 of 16 December 2021, 645 rectified by Decree n.3175 of 18 December 2021 of Italian Ministry of University and Research 646 funded by the European Union – Next Generation EU, and partially with financial support of the RETURN Extended Partnership and received funding from the European Union Next-GenerationEU (National Recovery and Resilience Plan – NRRP, Mission 4, Component 2, Investment 1.3 – D.D. 1243 2/8/2022, PE0000005). The authors would like to thank Prof. Vladimir Nikora (University of Aberdeen, UK) who was source of inspiration of the present study. Open access publishing facilitated by Universita degli Studi di Palermo, as part of the Wiley - CRUI-CARE agreement.

DATA AVAILABILITY STATEMENT

Data available on request from the authors.

ORCID

Donatella Termini https://orcid.org/0000-0003-3243-7103

REFERENCES

Ackerman, J.D. & Okumbo, A. (1993) Reduced mixing in a marine macrophyte canopy. *Functional Ecology*, 7, 305–309.

Afzalimehr, H., Riazi, P., Jahadi, M. & Singh, V.P. (2021) Effect of vegetation patches on flow structures and the estimation of friction factor. *ISH Journal of Hydraulic Engineering*, 27(sup1), 390–400. Available from: https://doi.org/10.1080/09715010.2019.1660920

Anderson, W., Barros, J.M., Christensen, K.T. & Awasthi, A. (2015) Numerical and experimental study of mechanisms responsible for turbulent secondary flows in boundary layer flows over spanwise heterogeneous roughness. *Journal of Fluid Mechanics*, 768, 316–347. Available from: https://doi.org/10.1017/jfm.2015.91

Bahmanpouri, F., Barbetta, S., Gualtieri, C., Ianniruberto, M., Filizola, N., Termini, D., et al. (2022) Prediction of river discharges at confluences based on entropy theory and surface-velocity measurements. *Journal of Hydrology*, 606, 127404. Available from: https://doi.org/10.1016/j.jhydrol.2021.127404

Barsu, S., Doppler, D., Jerome, J.J.S., Riviere, N. & Lance, M. (2016) Drag measurements in laterally confined 2D canopies: Reconfiguration and sheltering effect. *Physics of Fluids*, 28(10), 107101. Available from: https://doi.org/10.1063/1.4962309

Biggs, B.J. (1996) Hydraulic habitat of plants in streams. *Regulated Rivers: Research and Management*, 12(2–3), 131–144. Available from: https://doi.org/10.1002/(sici)1099-1646(199603)12:2/3<131::aid-rrr385>3.0.co;2-x

Biggs, H.J., Nikora, V., Gibbins, C., Cameron, S., Papadopoulos, K., Stewart, M., et al. (2019) Flow interactions with an aquatic macrophyte: A field study using stereoscopic particle image velocimetry. *Journal of Ecohydraulics*, 4(2), 113–130. Available from: https://doi.org/10.1080/24705357.2019.1606677

Blanckaert, K. (2010) Topographic steering, flow recirculation, velocity redistribution, and bed topography in sharp meander bends. *Water Resources Research*, 46(9), W09506. Available from: https://doi.org/10.1029/2009WR008303

Blanckaert, K. (2011) Processes in sharp meander bend sand their morphological implications bends. *Journal of Geophysical Research*, 116, F01003.

Blanckaert, K. & Graf, W.H. (2001) Mean flow and turbulence in open-channel bend. *Journal of Hydraulic Engineering*, 127(10), 835–847.

Bornette, G., Amoros, C. & Lamouroux, N. (1998) Aquatic plant diversity in riverine wetlands: The role of connectivity. *Freshwater Biology*, 39(2), 267–283. Available from: https://doi.org/10.1046/j.1365-2427.1998.00273.x

Bouma, T.J., van Duren, L.A., Temmerman, S., Claverie, T., Blanco-Garcia, A., Ysebaert, T., et al. (2007) Spatial flow and sedimentation patterns within patches of epibenthic structures: Combining field, flume and modelling experiments. *Continental Shelf Research*, 27(2007), 1020–1045.

Bywater-Reyes, S., Diehl, R.M. & Wilcox, A.C. (2018) The Influence of a Vegetated Bar on Channel-Bend Flow Dynamics – Data Set #1, in Earth Surface Dynamics Data Sets, University of Northern Colorado. Available from: https://digscholarship.unco.edu/esd_data_2018/1

Caffrey, J.M. & Kemp, W.M. (1992) Influence of the submersed plant, *Potamogeton perfoliatus*, on nitrogen cycling in estuarine sediments. *Limnology and Oceanography*, 37(7), 1483–1495.

Carollo, F.G., Ferro, V. & Termini, D. (2002) Flow velocity measurement in vegetated channels. *Journal of Hydraulic Engineering ASCE*, 128(7), 664–673.

Carollo, F.G., Ferro, V. & Termini, D. (2007) Analysing longitudinal turbulence intensity in vegetated channels. *Journal of Agricultural Engineering*, 4, 25–35.

Carollo, F.G., Ferro, V. & Termini, D. (2008) Flow velocity profile and turbulence characteristics in a vegetated straight flume. International Congress Riverflow 2008- Cesnme - Izmir (Turkey) 3-5 September 2008.

Chang, H. (1988) *Fluvial Processes in River Engineering*. New York: Wiley-Interscience publication, John Wiley and Sons.

Chang, K. & Constantinescu, G. (2015) Numerical investigation of _ow and turbulence structure through and around a circular array of rigid cylinders. *Journal of Fluid Mechanics*, 776, 161–199.

Chen, S.C., Kuo, Y.M. & Li, Y.H. (2011) Flow characteristics within different configurations of submerged flexible vegetation. *Journal of Hydrology*, 398(1), 124–134. Available from: https://doi.org/10.1016/j.jhydrol.2010.12.018

Chen, Z., Jiang, C. & Nepf, H.M. (2013) Flow adjustment at the leading edge of a submerged aquatic canopy. *Water Resources Research*, 49(9), 5537–5551. Available from: https://doi.org/10.1002/wrcr.20403

Cornacchia, L., Riviere, N., Soundar Jerome, J.J., Doppler, D., Vallier, F. & Puijalon, S. (2022) Flow and wake length downstream of live submerged vegetation patches: How do different species and patch configurations create sheltering in stressful habitats? *Water Resources Research*, 58(3), e2021WR030880. Available from: https://doi.org/10.1029/2021WR030880

Cornacchia, L., van de Koppel, J., van der Wal, D., Wharton, G., Puijalon, S. & Bouma, T.J. (2018) Landscapes of facilitation: How self-organized patchiness of aquatic macrophytes promotes diversity in streams. *Ecology*, 99(4), 832–847. Available from: https://doi.org/10.1002/ecy.2177.

Cotton, J., Wharton, G., Bass, J., Heppell, C. & Wotton, R. (2006) The effects of seasonal changes to in-stream vegetation cover on patterns of flow and accumulation of sediment. *Geomorphology*, 77(3), 320–334. Available from: https://doi.org/10.1016/j.geomorph.2006.01.010

Da Silva, A.M.F., El-Tahawy, T. & Tape, W.D. (2006) Variations of flow pattern with sinuosity in sine-generated meandering streams. *Journal of Hydraulic Enginnering*, 132(10), 1003–1014.

De Serio, F., Ben Meftah, M., Mossa, M. & Termini, D. (2018) Experimental investigation on dispersion mechanisms in rigid and flexiblevegetated beds. *Advances in Water Resources*, 120, 98–113.

Devi, T.B. & Kumar, B. (2016) Flow characteristics in an alluvial channel covered partially with submerged vegetation. *Ecological Engineering*, 94, 478–492. Available from: https://doi.org/10.1016/j.ecoleng.2016.06.018

Devi, T.B., Sharma, A. & Kumar, B. (2019) Flow characteristics in a partly vegetated channel with emergent vegetation and seepage. *Ecohydroly & Hydrobiology*, 19(1), 93–108. Available from: https://doi.org/10.1016/j.ecohyd.2018.07.006

Dietrich, W.E. & Smith, D. (1983) Influence of the point bar on flow through curved channels. *Water Resources Research*, 19(5), 1173–1192. Available from: https://doi.org/10.1029/wr019i005p01173

Figueiredo, B., Mormul, R. & Thomaz, S. (2015) Swimming and hiding regardless of the habitat: Prey fish do not choose between a native and a non-native macrophyte species as a refuge. *Hydrobiologia*, 746(1), 285–290.

Finotello, A., Ielpi, A., Lapôtre, M.G., Lazarus, E.D., Ghinassi, M., Carniello, L., et al. (2024) Vegetation enhances curvature-driven dynamics in meandering rivers. *Nature Communications*, 15(1), 1968. Available from: https://doi.org/10.1038/s41467-024-46292-x

Folkard, A.M. (2005) Hydrodynamics of model *Posidonia oceanica* patches in shallow water. *Limnology and Oceanography*, 50(5), 1592–1600. Available from: https://doi.org/10.4319/lo.2005.50.5.1592

Folkard, A.M. (2011) Vegetated flows in their environmental context: A review. *Proceedings of the Institution of Civil Engineers: Engineering and Computational Mechanics*, 164(EM1), 3–24. Available from: https://doi.org/10.1680/eacm.8.00006

Follett, E. & Nepf, H.M. (2012) Sediment patterns near a model patch of reedy emergent vegetation. *Geomorphology*, 179, 141–151. Available from: https://doi.org/10.1016/j.geomorph.2012.08.006

Fonseca, M., Ziema, J., Thayer, G. & Fisher, J. (1983) The role of current velocity in structuring eelgrass meadows. *Estuarine, Coastal and Shelf Science*, 17, 367–380.

Forman, R.T. (1995) *Land Mosaics: The Ecology of Landscapes and Regions*. Cambridge, UK: Cambridge University Press.

Franklin, P., Dunbar, M. & Whitehead, P. (2008) Flow controls on lowland river macrophytes: A review. *Science of the Total Environment*, 400(1), 369–378. Available from: https://doi.org/10.1016/j.scitotenv.2008.06.018

Gacia, E. & Duarte, C. (2001) Sediment retention by a Mediterranean *Posidonia oceanica* meadow: The balance between deposition and resuspension. *Estuarine, Coastal and Shelf Science*, 52(4), 505–514.

Ghisalberti, M. & Nepf, H.M. (2002) Mixing layer and coherent structures in vegetated acquatic flows. *Journal of Geophysical Research*, 107(2), 3-1–3-11.

Ghisalberti, M. & Nepf, H.M. (2006) The Structure of the Shear Layer in Flows over Rigid and Flexible Canopies. *Environmental Fluid Mechanics*, 6, 277–301. Available from: https://doi.org/10.1007/s10652-006-0002-4.

Hickin, E.J. (1977) Hydraulic factors controlling channel migration. Proc. of 5th Guelph Geomorphology Symposium- Geobooks, Norwich. U.K., 55–66.

Huai, W.-X., Li, S., Katul, G.G., Liu, M.-Y. & Yang, Z.-H. (2021) Flow dynamics and sediment transport in vegetated rivers: A review. *Journal of Hydrodynamics*, 33(3), 400–420. Available from: https://doi.org/10.1007/s42241-021-0043-7

Huai, W., Zeng, Y., Xu, Z. & Yang, Z. (2009) Three-layer model for vertical velocity distribution in open channel flow with submerged rigid vegetation. *Advances in Water Resources*, 32(4), 487–492.

Ielpi, A., Lapôtre, M.G.A., Gibling, M.R. & Boyce, C.K. (2022) The impact of vegetation on meandering rivers. *Nature Reviews Earth & Environment*, 3(3), 165–178. Available from: https://doi.org/10.1038/s43017-021-00249-6

Järvelä, J. (2002) Flow resistance of flexible and stiff vegetation: A flume study withnatural plants. *Journal of Hydrology*, 269(1), 44–54. Available from: https://doi.org/10.1016/s0022-1694(02)00193-2

Kazem, M., Afzalimehr, H. & Sui, J. (2021) Formation of Coherent Flow Structures beyond Vegetation Patches in Channel. *Water*, 13(20), 2812. Available from: https://doi.org/10.3390/w13202812

Killgore, K.J., Dibble, E.D. & Hoover, J.J. (1993) Relationships between Fish and Aquatic Plants: A Plan of Study; Miscellaneous Paper. U.S.Army Corps of Engineers: Vicksburg, MI, USA, pp. A-91–A-93.

Li, C., Huai, W. & Zeng, Y. (2013) Curved Open Channel Flow with Vegetation Roughened Outer Bank. Proceedings of 2013 IAHR World Congress

Li, Y.P., Wang, Y., Anim, D.O., Tang, C.Y., Du, W., Ni, L.X., et al. (2014) Flow characteristics in different densities of submerged flexible vegetation from an open-channel flume study of artificial plants. *Geomorphology*, 204, 314–324. Available from: https://doi.org/10.1016/j.geomo.rph.2013.08.015

Liu, C., Hu, Z., Lei, J. & Nepf, H. (2018) Vortex structure and sediment deposition in the wake behind a finite patch of model sub-merged vegetation. *Journal of Hydraulic Engineering*, 144(2), 04017065. Available from: https://doi.org/10.1061/(ASCE)HY.1943-7900.0001408

Liu, C., Shan, Y.Q., Liu, X.N., Yang, K.J. & Liao, H.S. (2016) The effect of floodplain grass on the flow characteristicsof meandering compound channels. *Journal of Hydrology*, 542, 1–17. Available from: https://doi.org/10.1016/j.jhydrol.2016.07.037

Liu, D., Diplas, P., Fairbanks, J.D. & Hodges, C.C. (2008) An experimental study of flowthrough rigid vegetation. *Journal of Geophysical Research*, 113(F4), 2008JF001042. Available from: https://doi.org/10.1029/2008JF001042

Liu, G., Zhang, Q., Wang, Y. & Liu, P. (2020) Application of water exchange physical model in artificial new port town. *IOP Conference Series:*

Earth and Environmental Science, 513, 012053. Available from: https://doi.org/10.1088/1755-1315/513/1/012053

Liu, Y. & Wang, P. (2024) Drag in vegetation canopy: Considering sheltering and blockage effects. *Water Resources Research*, 60(7), e2023WR036521. Available from: https://doi.org/10.1029/2023WR036521

Looby, A., Reynolds, L.K., Adams, C.R. & Martin, C.W. (2021) Submerged aquatic vegetation patch size affects fish communities in a turbid-algal lake. *Frontiers in Conservation Science*, 2, 12. Available from: https://doi.org/10.3389/fcosc.2021.657691

Lozovik, P.A., Zobkov, M.B., Borodulina, G.S. & Tokarev, I.V. (2019) Assessing external water exchange of lake bays by water chemistry characteristics. *Water Resources*, 46(1), 94–102. Available from: https://doi.org/10.1134/S0097.8078180501.23

Luhar, M. & Nepf, H.M. (2011) Flow-induced reconfiguration of buoyant and flexible aquatic vegetation. *Limnology and Oceanography*, 56(6), 2003–2017. Available from: https://doi.org/10.4319/lo.2011.56.6.2003

Manners, R.B., Wilcox, A.C., Kui, L., Lightbody, A.F., Stella, J.C. & Sklar, L.S. (2015) When do plants modify fluvial processes? Plant-hydraulic interactions under variable flow and sediment supply rates. *Journal of Geophysical Research: Earth Surface*, 120(2), 325–345. Available from: https://doi.org/10.1002/2014JF003265.

Mars, M., Kuruvilla, M. & Goen, H. (1999) The role of submergent macrophyte *triglochin huegelii* in domestic greywater treatment. *Ecological Engineering*, 12(1), 57–66.

Medjnoun, T., Vanderwel, C. & Ganapathisubramani, B. (2020) Effects of heterogeneous surface geometry on secondary flows in turbulent boundary layers. *Journal of Fluid Mechanics*, 886, 1–36. Available from: https://doi.org/10.1017/jfm.2019.1014

Nepf, H.M. (1999) Drag, turbulence, and diffusion in flow through emergent vegetation. *Water Resources Research*, 35(2), 479–489. Available from: https://doi.org/10.1029/1998WR900069

Nepf, H.M. (2012) Flow and transport in regions with aquatic vegetation. *Annual Review of Fluid Mechanics*, 44(1), 123–142. Available from: https://doi.org/10.1146/annurev-fluid-120710-101048

Nepf, H.M. & Vivoni, E. (2000) Flow structure in depth-limited, vegetated flow. *Journal of Geophysical Research*, 105(C12), 28547–28557. Available from: https://doi.org/10.1029/2000jc900145

Nezu, I. & Sanjou, M. (2008) Turbulence structure and coherent motion in vegetated canopy open-channel flows. *Journal of Hydro-Environment Research*, 2, 62–90.

Nikora, N., Nikora, V. & O'Donoghue, T. (2013) Velocity profiles in vegetated open channel flows: Combined effects of multiple mechanisms. *Journal of Hydraulic Engineering*, 139(10), 1021–1032.

Nikora, V. (2010) Hydrodynamics of aquatic ecosystems: An interface between ecology, biomechanics and environmental fluid mechanics. *River Research and Applications*, 26(4), 367–384. Available from: https://doi.org/10.1002/rra.1291

Nikora, V., Lamed, S., Nikora, N., Debnath, K., Cooper, G. & Reid, M. (2008) Hydraulic resistance due to aquatic vegetation in small streams: Field study. *Journal of Hydraulic Engineering*, 134(9), 1326–1332. Available from: https://doi.org/10.1061/(ASCE)0733-9429(2008)134:9(1326)

Okamoto, T.-A. & Nezu, I. (2013) Spatial evolution of coherent motions in finite-length vegetation patch flow. *Environmental Fluid Mechanics*, 13(5), 417–434. Available from: https://doi.org/10.1007/s10652-013-9275-6

Ortiz, S., Breidenbach, J. & Kändler, G. (2013) Early detection of bark beetle green attack using TerraSAR-X and RapidEye data. *Remote Sensing*, 5(4), 1912–1931. Available from: https://doi.org/10.3390/rs5041912

Pan, L., Jiang, R., Yang, X., Zhou, H., Cai, J., Li, N., et al. (2023) Experimental study on the disturbance effect of flexible vegetation patches of different shapes on slow-flow water body. *International journal of Environmental Science and Technology*, 20(3), 3133–3150. Available from: https://doi.org/10.1007/s13762-022-04166-z

Park, H. & Nepf, H. (2025) Turbulence in a channel with a patchy submerged canopy: the impact of spatial configuration. *Journal of Fluid Mechanics*, 1006, A15. Available from: https://doi.org/10.1017/jfm.2025.12.

Parker, G., Diplas, P. & Akiyama, J. (1983) Meander bends of high amplitude. *Journal of Hydraulic Engineering*, 109(10), 1323–1337, Available from: https://doi.org/10.1061/(ASCE)0733-9429(1983)109:10(1323)

Poggi, D., Porporato, A., Ridolfi, L., Albertson, J.D. & Katul, G.G. (2004) The effect of vegetation density on canopy sub-layer turbulence. *Boundary-Layer Meteorology*, 111(3), 565–587. Available from: https://doi.org/10.1023/B:BOUN.0000016576.05621.73

Przyborowski, Ł. & Łoboda, A.M. (2021) Identification of coherent structures downstream of patches of aquatic vegetation in a natural environment. *Journal of Hydrology*, 596, 126123. Available from: https://doi.org/10.1016/j.jhydrol.2021.126123

Przyborowski, Ł., Łoboda, A.M., Bialik, R.J. & Västilä, K. (2019) Flow field downstream of individual aquatic plants—Experiments in a natural river with *Potamogeton crispus* L. and *Myriophyllum spicatum* L. *Hydrological Processes*, 33(9), 1324–1337. Available from: https://doi.org/10.1002/hyp.13403

Rominger, J. & Nepf, H. (2011) Flow adjustment and interior flow associated with a rectangular porous obstruction. *Journal of Fluid Mechanics*, 680, 636–659.

Rowi'nski, M. & Kubrak, J. (2002) A mixing-length model for predicting vertical velocity distribution in flows through emergent vegetation. *Hydrological Sciences Journal*, 47, 893–904.

Sand-Jensen, K. & Pedersen, M.L. (2008) Streamlining of plant patches in streams. *Freshwater Biology*, 53(4), 714–726. Available from: https://doi.org/10.1111/j.1365-2427.2007.01928.x

Sand-Jensen, K. & Vindboek Madsen, T. (1992) Patch dynamics of the stream macrophyte, *Callitriche cophocarpa*. *Freshwater Biology*, 27(2), 277–282. Available from: https://doi.org/10.1111/j.1365-2427.1992.tb00539.x

Sand-Jensen, K. (1998) Influence of submerged macrophytes on sediment composition and near-bed flow in lowland streams. *Freshwater Biology*, 39(4), 663–679. Available from: https://doi.org/10.1046/j.1365-2427.1998.00316.x.

Schoelynck, J., Creelle, S., Buis, K., De Mulder, T., Emsens, W.-J., Hein, T., et al. (2018) What is a macrophyte patch? Patch identification in aquatic ecosystems and guidelines for consistent delineation. *Ecohydrology and Hydrobiology*, 18(1), 1–9. Available from: https://doi.org/10.1016/j.ecohyd.2017.10.005

Schoelynck, J., De Groote, T., Bal, K., Vandenbruwaene, W., Meire, P. & Temmerman, S. (2012) Self-organised patchiness and scale-dependent bio-geomorphic feedbacks in aquatic river vegetation. *Ecography*, 35(8), 760–768. Available from: https://doi.org/10.1111/j.1600-0587.2011.07177.x

Schulz, M., Kozerski, H., Pluntke, T. & Rinke, K. (2003) The influence of macrophytes on sedimentation and nutrient retention in the lower River Spree (Germany). *Water Research*, 37(3), 569–578. Available from: https://doi.org/10.1016/S0043-1354(02)00276-2

Siniscalchi, F., Nikora, V.I. & Aberle, J. (2012) Plant patch hydrodynamics in streams: Mean flow, turbulence and drag forces. *Water Resources Research*, 48(1), 2011WR011050. Available from: https://doi.org/10.1029/2011WR011050

Statzner, B., Gore, J.A. & Resh, V.H. (1988) Hydraulic stream ecology: Observed patterns and potential applications. *Journal of the North American Benthological Society*, 7(4), 307–360. Available from: https://doi.org/10.2307/1467296

Stone, B.M. & Shen, H.T. (2002) Hydraulic resistance of flow in channels with cylindrical roughness. *Journal of Hydraulic Engineering*, 128(5), 500–506. Available from: https://doi.org/10.1061/(asce)0733-9429(2002)128:5(500)

Sukhodolov, A. N., and Sukhodolova, T. A. (2006) Evolution of mixing layers in turbulent flow over submersed vegetation: Field experiments and measurement study. paper presented at the Internatl. Conf. on Fluvial Hydraulics (River Flow 2006), 6–8 September 2006, Lisbon, Portugal.

Sukhodolov, A.N. & Sukhodolova, T.A. (2010) Case study: Effect of submerged aquatic plants on turbulence structure in a lowland river. *Journal of Hydraulic Engineering*, 136(7), 434–446. Available from: https://doi.org/10.1061/(ASCE)HY.1943-7900.0000195

Sukhodolova, T.A. & Sukhodolov, A.N. (2012) Vegetated mixing layer around a finite-size patch of submerged plants. I: Theory and field experiments. *Water Resources Research*, 48(10), W10533.

Tan, C., Huang, B., Liu, D., Qiu, J., Chen, H., Li, Y., et al. (2019) Effect of Mimic Vegetation with Different Stiffness on Regular Wave Propagation and Turbulence. *Water*, 11(1), 109. Available from: https://doi.org/10.3390/w11010109

Tanino, Y. & Nepf, H. (2008) Lateral dispersion in random cylinder arrays at high reynods number. *Journal of Fluid Mechanics*, 600, 339–371.

Termini, D. (2009) Experimental observations of flow and bed processes in a large-amplitude meandering flume. *Journal of Hydraulic Engineering*, 135(7), 575–587.

Termini, D. (2015a) Flexible vegetation behavior and effects on flow conveyance: Experimental observations. *International Journal of River Basin Management*, 13(4), 401–411.

Termini, D. (2015b) Momentum transport and bed shear stress distribution in a meandering bend: Experimental analysis in a laboratory flume. *Advances in Water Resources*, 128, 128–141.

Termini, D. (2016) Experimental analysis of the effect of vegetation on flow and bed shear stress distribution in high-curvature bends. *Geomorphology*, 274C, 2016.

Termini, D. (2017) Vegetation effects on cross-sectional flow in a large amplitude meandering bend. *Journal of Hydraulic Research*, 55(3), 423–429. Available from: https://doi.org/10.1080/00221686.2016.1274918

Termini, D. (2019) Turbulent mixing and dispersion mechanisms over flexible and dense vegetation. *Acta Geophysica*, 67(3), 961–970. Available from: https://doi.org/10.1007/s11600-019-00272-8

Termini D. and Benistati N. (2022) Flexible vegetation distributed on the bed of the apex section of a meandering bend: an experimental study on the effect on the lateral dispersion. IRCBM 2022. Vol. 43. Technologies for Integrated River Basin Management p. 63-72 ISBN: 978-88-97181-86-6; ISSN 2282-5517- Edibios Cosenza (Italy)

Termini, D. & Di Leonardo, A. (2018) Turbulence structure and implications in exchange processes in high-amplitude vegetated meanders: Experimental investigation. *Advances in Water Resources*, 120, 114–127.

Termini, D. & Piraino, M. (2011) Experimental analysis of cross-sectional flow motion in a large amplitude meandering bend. *Earth Surface Processes and Landforms*, 36(2), 244–256. Available from: https://doi.org/10.1002/esp.2095

Termini, D. (2018) Experimental investigation of flow turbulent structure in a high-amplitude vegetated meandering laboratory flume. In: Armanini, A. & Nucci, E. (Eds.) *New Challenges in Hydraulic Research and Engineering: Proceedings of the 5th IAHR Europe Congress*. Trento, Italy: Research Publishing.

Tranmer, A.W., Ji, U., Ahn, M., Jung, S.H. & Yager, E.M. (2024) Characterizing erosion and deposition in and around riparian vegetation patches: Complex flow hydraulics, sediment supply, and morphodynamic feedbacks. *Water Resources Research*, 60(2), e2023WR034859. Available from: https://doi.org/10.1029/2023WR034859

Tseng, C.Y. & Tinoco, R.O. (2021) A Two-Layer Turbulence-Based Model to Predict. *Research Letters*, 48(3), e2020GL091255. Available from: https://doi.org/10.1029/2020GL091255.

Tseng, C.Y. & Tinoco, R.O. (2024) Canopy randomness, scale, and stem size effects on the interfacial transfer process in vegetated flows. *Water Resources Research*, 60, e2023WR035220. Available from: https://doi.org/10.1029/2023WR035220.

Vandenbruwaene, W., Temmerman, S., Bouma, T.J., Klaassen, P.C., de Vries, M.B., Callaghan, D.P., et al. (2011) Flow-interactionwithdynamicvegetationpatches: Implications for biogeomorphic evolution of a tidal landscape. *Journal of Geophysical Research*, 116(F1), F01008. Available from: https://doi.org/10.1029/2010JF001788

Vargas-Luna, A., Crosato, A. & Uijttewaal, W.S.J. (2015) Effects of vegetation on flow and sediment transport: Comparative analyses and validation of predicting models. *Earth Surface Processes and Landforms*, 40(2), 157–176. Available from: https://doi.org/10.1002/esp.3633

Vermaas, D., Uijttewaal, W. & Hoitink, A. (2011) Lateral transfer of streamwise momentum caused by a roughness transition across a shallow channel. *Water Resources Research*, 47(2), 2010WR010138. Available from: https://doi.org/10.1029/2010wr010138

Wang, J., He, G., Huang, L., Dey, S. & Fang, H. (2024) Drag force on submerged flexible vegetation in an open-channel flow. *Water Resources Research*, 60(10), e2023WR036879. Available from: https://doi.org/10.1029/2023WR036879

Wharton, G., Cotton, J.A., Wotton, R.S., Bass, J.A., Heppell, C.M., Trimmer, M., et al. (2006) Macrophytes and suspension-feeding invertebrates modify flows and fine sediments in the Frome and Piddle catchments, Dorset (UK). *Journal of Hydrology*, 330(1), 171–184. Available from: https://doi.org/10.1016/j.jhydrol.2006.04.034

White, B. & Nepf, H. (2007) Shear instability and coherent structures in shallow flow adjacent to a porous layer. *Journal of Fluid Mechanics*, 593, 1–32. Available from: https://doi.org/10.1017/S0022112007008415

White, D.C., Morrison, R.R. & Nelson, P.A. (2023) Experimental Observations of Floodplain Vegetation, Bedforms, and Sediment Transport Interactions in a Meandering Channel. *Journal of Geophysical Research: Earth Surface*, 128(9), e2023JF007136. Available from: https://doi.org/10.1029/2023JF007136

White, D.C., Morrison, R.R. & Nelson, P.A. (2025) Floodplain Vegetation Density Effects on Meandering Channel Flow Patterns and Channel-Floodplain Hydraulic Exchange. *Journal of Geophysical Research: Earth Surface*, 130(7), e2024JF008038. Available from: https://doi.org/10.1029/2024JF008038

Whiting, P.J. & Dietrich, W.E. (1993) Experimental studies of bed topography and flow patterns in large-amplitude meanders, 2. Mechanisms. *Water Resources Research*, 29(11), 3615–3622.

Whittaker, P., Wilson, C.A.M.E. & Aberle, J. (2015) An improved Cauchy number approach for predicting the drag and reconfiguration of flexible vegetation. *Advances inWater Resources*, 83(2015), 28–35. Available from: https://doi.org/10.1016/j.advwatres.2015.05.005

Widdows, J., Pope, N. & Brinsley, M. (2008) Effect of *Spartina anglica*stems on near-bed hydrodynamics, sediment erodability, and morphological changes on an intertidal mudflat. *Marine Ecology Progress Series*, 362, 45–57. Available from: https://doi.org/10.3354/meps07448

Wilcock, R., Champion, P., Nagels, J. & Crocker, G. (1999) The influence of aquaticmacrophytes on the hydraulic and physicochemical properties of a NewZealand lowland stream. *Hydrobiologia*, 416(1), 203–214.

Windham, L., Weis, J. & Weis, P. (2003) Uptake and distribution of metals in two dominant salt marsh macrophytes, *Spartina alterniflora* and *Phragmites australis*. *Estuarine, Coastal and Shelf Science*, 56, 63–72.

Wu, F.-C., Shen, H.-W. & Chou, Y.-J. (1999) Variation of roughness coefficients for unsubmerged and submerged vegetation. *Journal of Hydraulic Engineering*, 125(9), 934–942. Available from: https://doi.org/10.1061/(ASCE)0733-9429(1999)125:9(934)

Yalin, M.S. (1992) *River Mechanics*. London: Pregamon Press.

Yang, Y., Lin, Y.-T. & Ji, X. (2022) Hydrodynamic characteristics of flow over emergent vegetation in a strongly curved channel. *Journal of Hydraulic Research*, 60(2), 240–257. Available from: https://doi.org/10.1080/00221686.2021.1944920

You, X.Y. & Zhang, C.X. (2017) On improvement of water quality of a reservoir by optimizing water exchange. *Environmental Progress & Sustainable Energy*, 37(1), 399–409. Available from: https://doi.org/10.1002/ep.12693

Zhang, M., Li, C.W. & Shen, Y.M. (2013) Depth-averaged modeling of free surface flows in open channels with emerged and submerged vegetation. *Applied Mathematical Modelling*, 37(1–2), 540–553. Available from: https://doi.org/10.1016/j.apm.2012.02.049

Zhang, Y. & Nepf, H. (2025) Morphological change within and around a rectangular array of emergent vegetation is linked to flow structure. *Journal of Fluid Mechanics*, 1018, A37. Available from: https://doi.org/10.1017/jfm.2025.10492.

Zhao, T. & Nepf, H. (2024) Turbulence and bedload transport in submerged vegetation canopies. *Water Resources Research*, 60, e2024WR037694. Available from: https://doi.org/10.1029/2024WR037694.

Zhu, T., Cao, T., Ni, L., He, L., Yi, C., Yuan, C., et al. (2016) Improvement of waterquality by sediment capping and re-vegetation with *Vallisneria* *natans* L.: A short-term investigation using an in situ enclosure experiment in Lake Erhai, China. *Ecological Engineering*, 86, 113–119. Available from: https://doi.org/10.1016/j.ecoleng.2015.10.031

Zong, L. & Nepf, H. (2010) Flow and deposition in and around a finite patch of vegetation. *Geomorphology*, 116(3-4), 363–372. Available from: https://doi.org/10.1016/j.geomorph.2009.11.020

Zong, L. & Nepf, H. (2012) Vortex development behind a finite porous obstruction in a channel. *Journal of Fluid Mechanics*, 691, 368–391. Available from: https://doi.org/10.1017/jfm.2011.479

How to cite this article: Termini, D. & Benistati, N. (2026) Flexible patchy vegetation in a meandering bend: Effect on main flow and dispersion processes. *Earth Surface Processes and Landforms*, 51(3), e70271. Available from: https://doi.org/10.1002/esp.70271